Journal of Molecular Liquids 436 (2025) 128270

Contents lists available at ScienceDirect

Journal of Molecular Liquids

journal homepage: www.elsevier.com/locate/molliq

Exploring the potential of 1-ethyl-3-methylimidazolium octanoate–water systems as solvents for cellulose processing: Thermophysical and cytotoxicity insights

Rafael M. Almeida [a], Elitsa Gadeva [a,b], Ângela F.S. Santos [a], Rita Pacheco [a,c], Maria José V. Lourenço [a], Carlos Nieto de Castro [a,*]

[a] Centro de Química Estrutural, Institute of Molecular Sciences, Departamento de Química e Bioquímica, Faculdade de Ciências, Universidade de Lisboa, Campo Grande, 1749-016 Lisboa, Portugal
[b] Department of Physical Chemistry, Faculty of Chemistry, Paisii Hilendarski University of Plovdiv, Bulgaria
[c] Departamento de Engenharia Química, Polytechnic Institute of Lisbon, Av. Conselheiro Emídio Navarro, 1959-007 Lisboa, Portugal

ARTICLE INFO

Keywords:
1-Ethyl-3-Methylimidazolium Octanoate
Aqueous mixtures
Thermophysical properties
Cytotoxicity
HepG2 cells
Cellulose processing

ABSTRACT

The diverse applications of ionic liquids in the fields of chemistry, chemical engineering, medicine, and pharmacy necessitate a more comprehensive comprehension of the thermophysical and toxicological characteristics of potential new solvents and engineering fluids. The dissolution of cellulose and its subsequent applications in the textile industry indicated that $[C_2mim][C_7H_{15}COO]$, 1-Ethyl-3-Methylimidazolium Octanoate, and its mixtures with water have the potential to be highly efficient solvents with industrial applications.

This paper reports the first measurements of the density, speed of sound, thermal conductivity, and refractive index of 1-Ethyl-3-Methylimidazolium Octanoate and its mixtures with water in the temperature interval $283.15 < T/K < 348.15$, at 0.1 MPa. Because the ionic liquid and water are miscible, the mixture's whole composition range was investigated. Derived properties of the mixture, like the thermal expansion coefficient, the isobaric compressibility, intermolecular free length, and the excess volumes, were obtained and analysed. Results show similar behaviour with previous studies with other alkylimidazolium cations and anions, suggesting similar structural arrangements in the aqueous mixtures, with some particularities depending mostly on the anion chemical structure.

The thermal conductivity of pure ionic liquids and their aqueous mixtures cannot be semi-theoretically estimated using the Bridgman and Filaments model at present, as shown by molecular modelling. An empirical equation based on the dependence of thermal conductivity on the molecular mass previously developed could estimate the thermal conductivity of the ionic liquid to within 3.8 %.

The results obtained for the refractive index showed that the binary mixture could be considered ideal within the measurement uncertainty and that the ideal molar refraction is additive in terms of mole fractions, a result only demonstrated before for molecules of simple molecular constitution.

The cytotoxicity of this ionic liquid was assessed for the first time through in vitro studies in HepG2 cells, a human hepatic cell line widely accepted as a relevant model for evaluating the potential toxic effects of chemical agents and xenobiotics. Results obtained support its classification as a relatively safer imidazolium-based IL. An LC_{50} value of 9.2 mM was determined in HepG2 liver cells, indicating lower cytotoxicity compared to other ILs with longer alkyl chains on the cation.

1. Introduction

MacFarlane, Kar, and Pringle define ionic liquids (ILs) as "a liquid comprised entirely of ions", being salts in the liquid state. These compounds are some of the most promising fluids in chemistry and various applications. Composed of at least one cation and one anion, ILs have some relevant properties, like their high thermal stability, non-flammability, high electrical conductivity, and low vapor pressure

* Corresponding author.
E-mail address: cacastro@ciencias.ulisboa.pt (C. Nieto de Castro).

https://doi.org/10.1016/j.molliq.2025.128270
Received 8 May 2025; Received in revised form 30 July 2025; Accepted 31 July 2025
Available online 5 August 2025

over a wide range of temperatures, in some cases greater than the normal boiling point of water. The number of combinations of anions and cations in ILs is immense. As such, the IL can be designed for a target-oriented purpose. These compounds can be used as heat transfer and storage fluids, electrolytes in batteries, and as solvents in organic synthesis, and they can have medicinal and industrial applications [1–5].

Many authors have described ILs as environmentally friendly solvents [1,2,5–7]. However, several studies have demonstrated the toxicity of various ILs toward different biological systems, including animals, plants, and microorganisms, along with the potential to cause environmental effects on soil and aquatic ecosystems. A recent review on their toxicity to living organisms [8] shows that the available data is still scarce, the existing tests incomplete, and conclusions difficult to harmonize. However, it is now widely recognized that the safety and environmental impact of ILs depend on the specific nature of the IL and the conditions of their application [9].

One of the most recent applications of ILs is on the dissolution of cellulose, the most abundant biopolymer on the planet, and one of the most important raw materials in the fiber industry [10]. In this review, it is said that, "based on the limitations of cellulose in terms of dissolution/processing, and focused on green chemistry, new cellulose production techniques are emerging, such as dissolution and functionalization in ionic liquids, in processing cellulose, including pretreatment, hydrolysis, functionalization, and conversion into bio-based platform chemicals." 1-Ethyl-3-methylimidazolium acetate, [C_2mim][CH_3COO], has shown a good solvent capacity, and some studies show that 1-ethyl-3-methylimidazolium octanoate, [C_2mim][C_7H_{15}COO], can be used to dissolve this polymer, with the same success [11,12].

Although our group had already studied the properties of [C_2mim][CH_3COO] [13], and despite the promising qualities already mentioned, there have been few experimental measurements of ILs' thermal properties, and none for [C_2mim][C_7H_{15}COO]. Using this compound as a solvent in any chemical process, like extraction, more data on its thermophysical properties are necessary for a deeper understanding of these fluids, their molecular interactions in the liquid state, making them a more viable option for several applications.

New and unique data on the density, speed of sound, refractive index, and thermal conductivity of the pure ionic liquid [C_2mim][C_7H_{15}COO], and of its mixtures with water for large composition and temperature ranges, are reported in the present work. Additionally, the cytotoxicity of this ionic liquid was assessed through in vitro studies in HepG2 cells, a human hepatic cell line widely accepted as a relevant model for evaluating the potential toxic effects of chemical agents and xenobiotics [14].

2. Experimental

2.1. Materials

1-Ethyl-3-methylimidazolium octanoate, [C_2mim][C_7H_{15}COO], (CAS N# 1154003–55-0) was purchased from IoLiTec (Product N# IL-0357-HP), Ionic Liquids Technologies, Germany, and the product specifications of the certificate analysis are described in Table 1. Dulbecco's Modified Eagle Medium (DMEM) and fetal bovine serum (FBS) were obtained from Biowest. Trypsin and glutamine were purchased from Biowhittaker® Lonza. Phosphate-buffered saline (PBS) was obtained from Corning (Corning, NY, USA). Antibiotic–antimycotic solution 100 × (10,000 U/mL penicillin, 10 mg/mL streptomycin, and 25 μg amphotericin B/mL), (4,5-dimethylthiazol-1-yl)-2,5-diphenyltetrazolium (MTT) were obtained from VWR (Radnor, PA, USA).

To the best authors' knowledge, supported by database searches, there are no literature data sets available for the reported properties of the "pure" [C_2mim][C_7H_{15}COO] or its mixtures with water to compare with, nor has the cytotoxicity of this ionic liquid been assessed through in vitro studies in HepG2 cells. Therefore, the data reported in this work are unique, obtained for the first time.

2.2. Sample preparation

The ionic liquid was dried under vacuum, at 70 °C, for 48 h, and sealed in a flask for further measurements of its properties. The water content was determined by Coulometric Karl Fischer titration (Metrohm 831). For the preparation by weight of the mixtures with water, the mass was measured using a Kern AEJ balance with a standard uncertainty of 1×10^{-5} g, considering the residual water content of the "pure" ionic liquid in the assignment of the mass/mole fractions of each mixture. Mixtures were prepared with Milli-Q® water.

Table 2 shows the amount of water in each sample of the pure ionic liquid, before the measurements, and used for the preparation of the [C_2mim][C_7H_{15}COO] + water mixtures. Although several trials in drying were made, it was not possible to decrease more the initial water content of the ionic liquid, except for the refractive index batch, whereby we achieved a value almost three times smaller than the others, by using low-volume liquid flasks in the drying rig. The final mole fraction of the mixtures studied considered this initial water content of the ionic liquid. The relative combined standard uncertainty in the mixture composition, expressed in mole fraction, was found to be $u_{r,c}(x_{IL}) = 0.002$.

2.3. Methods of measurements

2.3.1. Density and speed of sound

The measurements of density, ρ, and speed of sound, c, were performed with an Anton Paar density and speed of sound meter DSA 5000 M, with an automatic temperature control within ±0.001 K and a standard uncertainty $u(T) = 0.01$ K, for a temperature range $283.15 < T/K < 343.15$. Due to the high viscosity of the mixtures, density values were corrected for this extra damping, following the densimeter manufacturer's recommendations, which estimates the viscosity of the sample from programmed experiments of overtones detection. As no measurements of viscosity exist, the manufacturer's automatic correction has to be assumed as acceptable. Details of the calibrations performed can be found in recent publications [15–18].

Calibration of the speed of sound cell (frequency of the ultrasound

Table 2
Water content in [C_2mim][C_7H_{15}COO] samples used for mixture preparation.

Sample[a]	w_w /ppm
Density	19,927 ± 313
Speed of sound	19,927 ± 313
Thermal Conductivity	19,927 ± 313
Refractive Index	7,269 ± 86

[a] Batch V001x98.12-CS-1330.

Table 1
Material specifications.

	Identity (NMR. IR)	Assay (NMR)	Cation (IC)	Anion (IC)	Halides (IC)	Water (KF)/ppm[a]	Appearance	Date
[C_2mim][C_7H_{15}COO] Batch: V001x98.12-CS-1330	pass	> 95 %	≥98 %	≥98 %	<50 ppm	37,000	slightly yellow liquid	2023.05.23

[a] measurement in the laboratory upon reception.

transducer is close to 3 MHz) was made according to the manufacturer's recommendation, and a correction to the values was made as explained in other works by our group [17–20] and briefly described here. Before measuring the speed of sound of any mixture, the speed of sound of water at each temperature, $c_{0,exp}$, has been measured at the operating frequency of the instrument, 3 MHz. As these values do not always reproduce the reference value $c_{0,ref}$ at each temperature, differences ($c_{0,exp}$ - $c_{0,ref}$) were estimated and $c_{0,ref}$ was added to that difference, thus eliminating any systematic deviation. The true c value (reported in Table 7) is then

$c\ (T,\ x_w) = (c_{exp}$ - $c_{0,exp}) + c_{0,ref}\ (T,\ x_w)$. The possible existence of ultrasound absorption, which would influence the reproducibility of the measurements, was not found.

The density of pure water was measured, and the results are compared with the values present in the literature [21,22]. Data obtained did not deviate from the standard reference data value by more than 0.05 kg·m^{-3}, within the uncertainty of the densimeter. The standard uncertainties of density and speed of sound measurements are then estimated to be $u\ (\rho) = 0.30$ kg·m^{-3} and $u\ (c) = 0.5$ m·s^{-1}, respectively. The expanded global uncertainty, at a 95 % confidence level ($k = 2$), is $U\ (\rho) = 0.60$ kg·m^{-3} and $U\ (c) = 1.0$ m·s^{-1}.

2.3.2. Thermal conductivity

The measurements of the thermal conductivity, λ,of [C_2mim][C_7H_{15}COO] and its aqueous mixtures were performed at temperatures $288.15 < T/K < 348.15$, at atmospheric pressure, using commercial equipment from Hukseflux Thermal Sensors TPSYS02 and a Non-Steady-State Probe (NSSP) TP08, SN# 283, with a temperature standard uncertainty of $u(T) = 0.02$ K.

Before the measurements, it was necessary to assess the quality of the methodology. To do this, the thermal conductivity of the water was measured, and the results are compared with the values obtained by the IUPAC SRD correlation [23]. Five experimental values were obtained for each temperature defined in the exterior thermostat bath. Data obtained between 280 and 350 K did not deviate from the standard reference data value by more than 0.6 %. Data for different power inputs showed no indication of convection in the cell, proving, along with results obtained for other ionic liquids reported elsewhere [16–18,24–26], that the theory of the transient hot-wire technique [24] could be used to obtain rigorous values of thermal conductivity of the ionic liquid and its mixtures with water. Data obtained have an estimated expanded relative global uncertainty $U_r\ (\lambda) = 0.02$, at a 95 % confidence level ($k = 2$).

2.3.3. Refractive index

The measurements of the refractive index for sodium D line (589.26 nm), n^D, were performed at atmospheric pressure, for $283.15 < T/K < 343.15$ K, with an Anton Paar (Abbemat 500) refractometer, with direct experimental values corrected by calibration, described in a previous publication [13]. This model of refractometer uses only the calibration at 293.15 K, with data for water. When measuring the refractive index for higher temperatures, a systematic difference was found, in comparison with the reference data of Marsh (1987) [27]. Calibration was further checked with n-hexadecane, using data from reference [27] and Sirbu et al. (2019) [28]. The systematic deviations were regressed as a function of temperature and applied to the current experimental measurements. The corrections have to be applied, especially above 313 K, as they are bigger than the uncertainty of the refractometer, although not greater than – 0.0003 RI units, at the highest temperature. Temperature was measured with an uncertainty of 0.03 K, and the expanded global uncertainty in the refractive index is $U\ (n) = 0.0002$, at a 95 % confidence level ($k = 2$).

2.3.4. Cytotoxicity

The HepG2 cell line (ECACC catalogue no. 85011430) was obtained from the European Collection of Authenticated Cell Cultures (ECACC) biobank and cultured according to the supplier's guidelines. Cells were maintained in DMEM (Dulbecco's Modified Eagle's Medium), supplemented with 10 % fetal bovine serum (FBS) and 1 % antibiotic-antimycotic, in a humidified atmosphere with 5 % CO2 at 37 °C. Subculturing was performed when cultures reached 80–85 % confluence, following the biobank's instructions. The viability of HepG2 cells was assessed after 24-h exposure to varying concentrations of [C2mim][C7H15COO], ranging from 3 to 30 mM. The 3-(4,5-dimethylthiazol-2-yl)-2,5-diphenyltetrazolium bromide (MTT) colorimetric assay was conducted as previously described protocols [29].

Briefly, 50×10^3 HepG2 cells were seeded per well in 96-well plates and incubated at 37 °C in an atmosphere with 5 % CO2 for approximately 48 h until they reached confluence. The medium was then replaced with various concentrations of the [C2mim][C7H15COO] solution in DMEM, along with a negative control group incubated only in DMEM. Each concentration and control were tested in 6 replicates. After 24 h of incubation under the same conditions, the medium was replaced with 0.05 mg/mL MTT reagent in DMEM, and the cells were incubated for an additional 2 h or until the formation of the formazan crystals was achieved. The MTT solution was removed and replaced with 200 μL of methanol per well to dissolve the crystals. Absorbance was measured at 595 nm, with a reference wavelength of 630 nm. The percentage of cell viability for each concentration was calculated, with 100 % viability corresponding to the control group. The results were expressed as the percentage of cell death. The concentration of [C2mim][C7H15COO] that resulted in 50 % cell death (LC50) was estimated.

3. Results

3.1. Density, isobaric thermal expansion and excess molar volume

The values for the density, ρ, were measured at atmospheric pressure for $283.15 < T\ /\ K < 343.15$, and are shown in Table 3 and represented in Fig. 1. Density decreases with temperature increase and increases with the mole fraction of water until $x_w \approx 0.86$, decreasing as it approaches the values of pure water. With the data of a previous work from our group regarding the density of [C_2mim][CH_3COO] [13], it can be seen that [C_2mim][C_7H_{15}COO] has a lower density, suggesting that density decreases with the increase of the anions' alkyl chain, as is predictable. Although it is well established that the increase of the cations' alkyl chain decreases the density of the IL [30,31], probably due to a worse packing efficiency, it is not the case regarding the anions' alkyl chain. While some authors state that the density increases with the molecular weight of the anion [32,33], other studies don't follow the same trend [34–36]. In this way, more studies regarding the density of ILs containing the same cation, namely for [C_2mim][C_nH_{2n+1}COO] systems, are necessary.

The water-free values for the density of [C_2mim][C_7H_{15}COO] were obtained by fitting the four experimental values closer to $x_{IL} = 1$ as a quadratic function of the mole fraction of the ionic liquid, and then by extrapolating to $x_{IL} = 1$. The extrapolated water-free values of the density of the ionic liquid, ρ_{wf} are also presented in the last line of Table 3 and shown in Fig. 1. The water-free data can be correlated by Eq. (1):

$$\rho_{wf}\left(\mathrm{kg} \bullet \mathrm{m}^{-3}\right) = a_1 + a_2 \times (T/\mathrm{K}) + a_3 \times (T/\mathrm{K})^2 \quad (1)$$

with coefficients $a_1 = (13{,}357 \pm 28)$ kg·m^{-3}, $a_2 = (-1.582 \pm 0.179)$ kg·m^{-3}·K^{-1} and $a_3 = (0.0015 \pm 0.0003)$ kg·m^{-3}·K^{-2}. The standard deviation of the fit is 0.27 kg·m^{-3} and no point deviates by more than 0.44 kg·m^{-3}.

It was possible to fit the experimental results, for each temperature, to polynomial equations of the type of Eq. (2):

$$\rho(x_w, T) \Big/ \mathrm{kg{\cdot}m^{-3}} = \sum_{i=0}^{i=7} a_i(T) x_w^i \quad (2)$$

Table 3
Density[a], ρ, for $[C_2mim][C_7H_{15}COO] + H_2O$, in the temperature range $T = (283.15$ to $343.15)$ K[b] and $P = 0.1$ MPa[b], as a function of the mass fraction of water, w_w, and of the mole fraction of the ionic liquid, x_{IL}.

w_w	x_{IL}[c]	ρ / kg·m^{-3}								
		283.15 K	288.15 K	293.15 K	298.15 K	303.15 K	313.15 K	323.15 K	333.15 K	343.15 K
1.000	0.000	999.70	999.10	998.20	997.00	995.70	992.20	988.00	983.20	977.80
0.980	0.001	1000.77	1000.08	999.09	997.85	996.38	992.82	988.52	983.57	978.07
0.950	0.004	1002.58	1001.72	1000.58	999.21	997.61	993.81	989.31	984.18	978.50
0.900	0.008	1005.73	1004.49	1003.01	1001.33	999.46	995.22	990.38	984.98	979.08
0.800	0.017	1009.69	1007.88	1005.93	1003.85	1001.64	996.83	991.54	985.81	979.64
0.650	0.037	1014.62	1012.27	1009.82	1007.28	1004.65	999.14	993.29	987.10	980.59
0.500	0.066	1019.61	1016.75	1013.85	1010.89	1007.88	1001.71	995.33	988.74	981.93
0.300	0.142	1024.65	1021.38	1018.09	1014.79	1011.48	1004.80	998.03	991.17	984.19
0.225	0.196	1024.21	1020.95	1017.65	1014.36	1011.05	1004.42	997.73	990.98	984.17
0.106	0.375	1019.60	1016.47	1013.18	1010.01	1006.83	1000.43	994.02	987.60	981.15
0.050	0.574	1014.35	1011.23	1007.38	1004.29	1001.20	995.05	988.84	982.63	976.44
0.021	0.772	1010.29	1007.18	1003.31	999.98	996.90	990.58	984.44	978.32	972.22
0.000[d]	1.000[d]	1005.97	1002.8	998.56	994.80	991.65	984.95	978.75	972.55	966.38

[a] Expanded global uncertainty, $U(\rho) = 0.60$ kg·m^{-3}, at a 95 % confidence level ($k = 2$)
[b] Standard uncertainty, $u(T) = 0.01$ K, $u(P) = 0.002$ MPa
[c] Relative combined standard uncertainty, $u_{r,c}(x_w) = 0.002$
[d] Extrapolated water-free value.

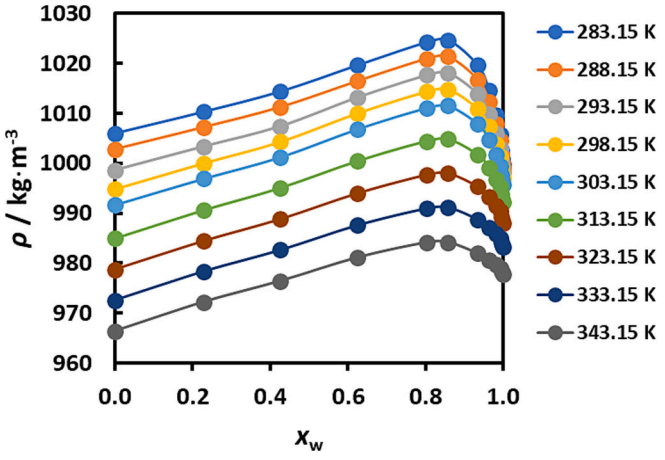

Fig. 1. Density, ρ, for the system $[C_2mim][C_7H_{15}COO] + H_2O$ as a function of x_w, for the temperatures studied.

The value of i was optimized for a minimum standard deviation, and it was found that $i = 7$ produced the best fit. The values of the coefficients and the standard deviation of the fits are presented in Table 4. No point deviates by more than ±0.1 %, around 1 kg·m^{-3}.

Having the data for the variation of the density at different temperatures, as a function of composition, the isobaric thermal expansion coefficient can be calculated for each composition, α_P, according to Eq. (3). The values can be found in Table 5 and displayed in Fig. 2.

$$\alpha_P(T,x) = -\frac{1}{\rho(T,x)}\left(\frac{\partial\rho(T,x)}{\partial T}\right)_{P,x} \quad (3)$$

According to Fig. 2, thermal expansion did not exhibit significant variation with temperature. Regarding the composition dependence, it stays almost constant up to $x_w \approx 0.9$, where it starts to decrease as the mixture composition approaches pure water, probably due to a possible change of structure in the liquid mixture occurring, namely in its nanoscopic organization, as discussed previously in another study performed by our group [17,18].

It is clear from this figure that the thermal expansion coefficient does not vary much with temperature, and that the behaviour for water-rich mixtures does not depend on temperature, as found for previous systems studied, with the anions $[CH_3SO_3]$ and $[N(CN)_2]$ [17,18]. This might be a consequence of the fact that the long octyl chain, making the structure less compact, allows for a better acceptance the presence of water molecules.

The excess molar volume of the mixtures represents the difference between the measured molar volume and that expected based on the simple addition of the two pure components, and can be calculated using Eq. (4):

$$V_m^E = \frac{M_w x_w + M_{IL} x_{IL}}{\rho} - x_w\frac{M_w}{\rho_w} - x_{IL}\frac{M_{IL}}{\rho_{IL}} \quad (4)$$

where M_i and ρ_i are the molecular weights and density of the pure components, w for water and IL for $[C_2mim][C_7H_{15}COO]$. The values can be found in Table 6 and displayed in Fig. 3.

For this system, the excess molar volumes are always negative, decreasing with temperature. A possible (negative) minimum is achieved between $x_w \approx 0.42$ (at the higher temperatures) and $x_w \approx 0.64$ (at the lowest temperature), temperature dependent. The variation with composition is more symmetric at higher temperatures (see inset in Fig. 3). The estimated standard uncertainties of the mole fractions and the excess volumes are, respectively, $u_{r,c}(x_{IL}) = 0.002$ and $u(V_m^E) = 0.02$

Table 4
Coefficients of polynomial equations for the density variation with mole fraction and temperature, and the standard deviation, σ,of the fits.

T / K	283.15	288.15	293.15	298.15	303.15	313.15	323.15	333.15	343.15
a_0	1005.97	1002.78	998.560	994.803	991.654	984.950	978.748	972.549	966.384
a_1	−1467.95	−1226.71	−937.315	−773.917	−593.834	−389.511	−219.633	−71.3896	63.5711
a_2	17,537.4	−1467.95	1005.97	9457.99	7340.46	4933.47	2931.02	1187.69	−397.532
a_3	−80,173.6	−67,252.0	−52,319.4	−43,550.5	−33,888.1	−22,782.3	−13,605.9	−5631.13	1609.39
a_4	184,823	155,099	121,395	101,082	78,853.9	52,977.9	31,734.7	13,306.7	−3395.30
a_5	−229,215	−192,419	−151,463	−126,161	−98,666.6	−66,232.7	−39,745.7	−16,816.0	3920.97
a_6	146,317	122,876	97,244.1	81,040.0	63,551.3	42,637.5	25,627.8	10,935.6	−2317.23
a_7	−37,826.7	−31,784.7	−25,288.1	−21,091.2	−16,592.5	−11,136.6	−6712.54	−2900.51	527.816
σ / kg·m·$^{-3}$	0.94	0.84	0.78	0.71	0.64	0.54	0.46	0.38	0.31

Table 5
Isobaric thermal expansion[a], α_P, for $[C_2mim][C_7H_{15}COO] + H_2O$, in the temperature range $T = (283.15$ to $343.15)$ K[b] and $P = 0.1$ MPa[b], as a function of the mole fraction of water, x_w[c].

x_w	$\partial\rho/\partial T$	$10^4\ \alpha_P$ / K^{-1}								
		283.15 K	288.15 K	293.15 K	298.15 K	303.15 K	313.15 K	323.15 K	333.15 K	343.15 K
1.000	−0.37	3.67	3.67	3.67	3.68	3.68	3.70	3.71	3.73	3.75
0.999	−0.38	3.80	3.80	3.80	3.81	3.81	3.83	3.84	3.86	3.88
0.996	−0.40	4.01	4.02	4.02	4.03	4.03	4.05	4.07	4.09	4.11
0.992	−0.44	4.42	4.43	4.43	4.44	4.45	4.47	4.49	4.52	4.54
0.983	−0.50	4.95	4.96	4.97	4.98	4.99	5.02	5.04	5.07	5.10
0.963	−0.57	5.58	5.59	5.61	5.62	5.64	5.67	5.70	5.74	5.77
0.934	−0.63	6.15	6.17	6.19	6.20	6.22	6.26	6.30	6.34	6.39
0.858	−0.67	6.57	6.59	6.61	6.64	6.66	6.70	6.75	6.79	6.84
0.804	−0.67	6.51	6.53	6.55	6.57	6.60	6.64	6.68	6.73	6.78
0.625	−0.64	6.29	6.30	6.32	6.34	6.36	6.41	6.45	6.49	6.53
0.426	−0.63	6.20	6.22	6.24	6.26	6.28	6.32	6.36	6.40	6.44
0.228	−0.63	6.27	6.29	6.31	6.33	6.35	6.39	6.43	6.47	6.51
0.000[d]	−0.66	6.55	6.57	6.60	6.63	6.65	6.69	6.74	6.78	6.82

[a] Expanded global uncertainty, $U(\alpha_P) = 2 \times 10^{-6}$ K^{-1}, at a 95 % confidence level ($k = 2$)
[b] Standard uncertainty, $u(T) = 0.01$ K, $u(P) = 0.002$ MPa
[c] Relative combined standard uncertainty, $u_{r,c}(x_w) = 0.002$
[d] Extrapolated water-free value.

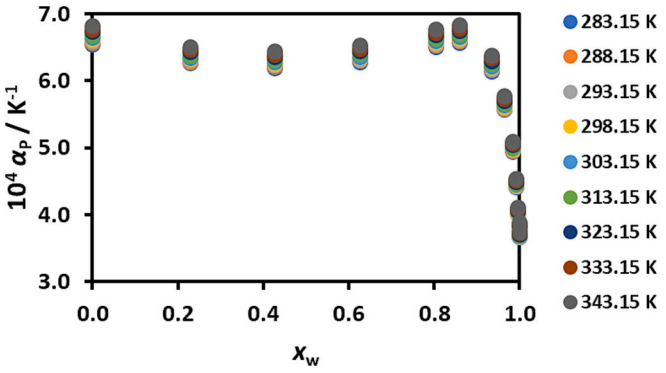

Fig. 2. Isobaric thermal expansion, α_P, for the aqueous $[C_2mim][C_7H_{15}COO]$ system, for the temperatures studied, as a function of x_w.

cm^3·mol^{-1}. These negative values are consistent with the excess molar volumes of other ionic liquids containing the same cation, namely $[C_2mim][CH_3COO]$ and $[C_2mim][CH_3SO_3]$. Unlike these ionic liquids, $[C_2mim][N(CN)_2]$ has a positive excess molar volume. A positive or negative excess molar volume can be due to the intermolecular interactions between the ions and the water, and a negative value suggests that the ions in the mixture can pack in a more efficient way than in their pure state, possibly reflecting, as it happens in most cases, an attractive behaviour between those molecular species [14,17,18]. Only data on excess enthalpy in this system can prove this assumption definitively.

The excess volume data (13 data points for each temperature) was correlated using the Redlich–Kister (RK) fitting method, Eq. (5). Results are also displayed in Fig. 3 as full lines.

$$V_m^E = x_w(1-x_w)\sum_{j=0}^{j=2,3,4} A_k(1-2x_w)^j \quad (5)$$

The number of A_j parameters has been optimized using the F-test, and they are displayed in Table S1, together with the respective standard uncertainties and the standard deviation of the fits.

For $T = 288.15$ and 288.15 K, 3 parameters were used ($j = 2$), and 4 parameters for the other temperatures ($j = 3$), except for $T = 343.15$ K, 5 parameters were necessary ($j = 4$). The standard deviation (at 95 % confidence level) of the fits does not exceed 0.02 cm^3·mol^{-1}, with no point deviating by more than 0.01 cm^3·mol^{-1}.

Table 6
Excess molar volume[a], V_m^E, for the aqueous system $[C_2mim][C_7H_{15}COO]$ from $T = (283.15$ to $343.15)$ K[b], at $P = 0.1$ MPa[b], as a function of the mole fraction of water, x_w[c].

x_w	V_m^E / cm^3·mol^{-1}								
	283.15 K	288.15 K	293.15 K	298.15 K	303.15 K	313.15 K	323.15 K	333.15 K	343.15 K
1.000	0.0000	0.0000	0.0000	0.0000	0.0000	0.0000	0.0000	0.0000	0.0000
0.999	−0.0173	−0.0166	−0.0163	−0.0165	−0.0141	−0.0142	−0.0133	−0.0111	−0.0096
0.996	−0.0484	−0.0459	−0.0447	−0.0439	−0.0402	−0.0379	−0.0344	−0.0297	−0.0253
0.992	−0.1068	−0.0993	−0.0947	−0.0905	−0.0832	−0.0755	−0.0672	−0.0587	−0.0506
0.983	−0.1913	−0.1767	−0.1688	−0.1612	−0.1498	−0.1364	−0.1224	−0.1089	−0.0960
0.963	−0.3344	−0.3133	−0.3043	−0.2939	−0.2772	−0.2562	−0.2332	−0.2114	−0.1906
0.934	−0.5523	−0.5231	−0.5141	−0.5010	−0.4774	−0.4469	−0.4118	−0.3790	−0.3479
0.858	−1.0302	−0.9927	−0.9957	−0.9863	−0.9553	−0.9190	−0.8694	−0.8231	−0.7783
0.804	−1.2309	−1.1970	−1.2153	−1.2164	−1.1873	−1.1605	−1.1138	−1.0710	−1.0301
0.625	−1.4877	−1.4740	−1.5455	−1.5895	−1.5745	−1.5921	−1.5667	−1.5457	−1.5247
0.426	−1.3093	−1.3088	−1.3500	−1.4420	−1.4458	−1.5266	−1.5276	−1.5350	−1.5434
0.228	−0.8772	−0.8897	−0.9508	−1.0348	−1.0462	−1.1254	−1.1440	−1.1693	−1.1959
0.000	0.0000	0.0000	0.0000	0.0000	0.0000	0.0000	0.0000	0.0000	0.0000

[a] Expanded global uncertainty, $U(V_m^E) =$ cm^3 mol^{-1}, at a 95 % confidence level ($k = 2$)
[b] Standard uncertainty, $u(T) = 0.01$ K, $u(P) = 0.002$ MPa
[c] Relative combined standard uncertainty, $u_{r,c}(x_w) = 0.002$.

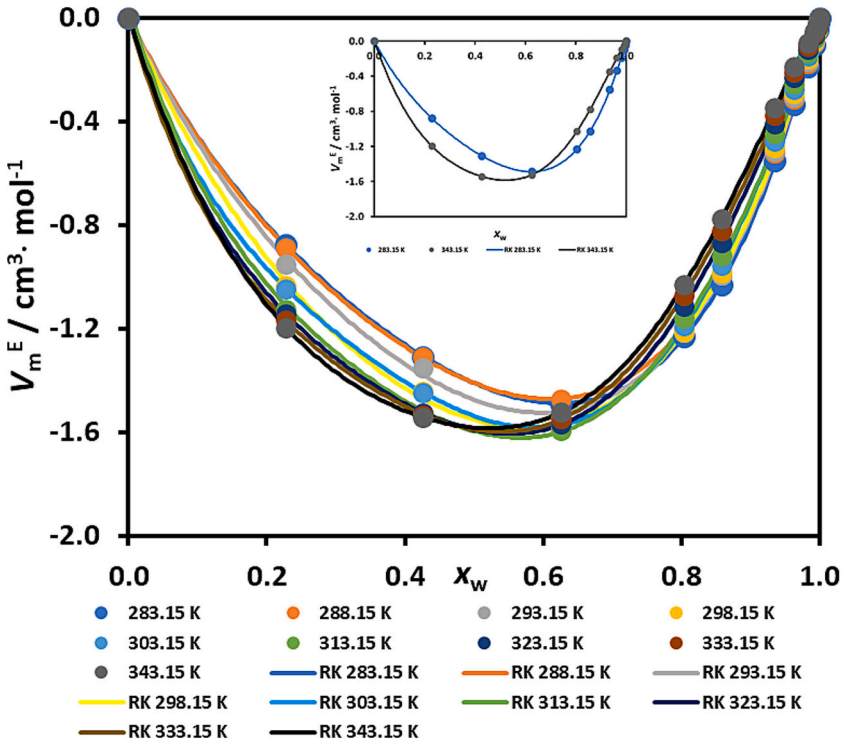

Fig. 3. Excess molar volumes, V_m^E, for the aqueous [C_2mim][C_7H_{15}COO] system, at the studied temperatures, as a function of x_w. Full lines stand for 3rd-degree Redlich-Kister fitting curves, except 2nd degree at T = 283.15 K and 288.15 K, and 4th degree, T = 343.15 K.

3.2. Speed of sound and isobaric compressibility. The Intermolecular free length

The measured values for the speed of sound for the system [C_2mim][C_7H_{15}COO] + water are all shown in Table 7 and displayed in Fig. 4. The values corresponding to pure water were those obtained for the cell calibration, based on the NIST Chemistry Webbook [37]. However, the values for the two lowest temperatures had to be calculated from Wagner and Kruse IAPWS equation of state [38], by correlating the difference between the two sets of data between 293 and 343 K and extrapolating the value to be applied to W&K data to estimate de value for NIST speed of sound data. More details can be found in the Supplementary Material, Table S2, and Fig. S1. The root mean square deviation of the fit is 0.11 m·s^{-1}, a value which is commensurate with the uncertainty of the calibration.

It is possible to observe from Fig. 4 that the speed of sound increases smoothly with the mole fraction of water until $x_w \approx 0.9$, where it reaches a maximum and decreases after it, as it approaches the values of pure water. This maximum is also present on the measurements our group has performed of the binary systems [C_2mim][CH_3COO] and [C_2mim][CH_3SO_3] with water, whereas it is not seen on [C_2mim][$C(CN)_2$] and [C_4mpyr][$C(CN)_2$] and might be due to a given interaction between the ions and the water molecules [13,16,17,36]. The speed of sound decreases with the increase of temperature, as expected and already explained in another work [22]. There is an inversion of the temperature coefficient after the maximum, for very diluted concentrations, which was already noted for all the systems mentioned above and might be due to a possible change of the molecular structure of the solutions already discussed. This can be better seen if we plot the speed of sound as a function of the mass fraction of water, as shown in Fig. S2, where the

Table 7
Speed of sound[a], c, for the aqueous system [C_2mim][C_7H_{15}COO] from T = (283.15 to 343.15) K[b], at P = 0.1 MPa[b], as a function of the mole fraction of water, x_w.

x_w[c]	c / m s^{-1}								
	283.15 K	288.15 K	293.15 K	298.15 K	303.15 K	313.15 K	323.15 K	333.15 K	343.15 K
1.000	1447.28	1465.86	1482.30	1496.70	1509.20	1528.90	1542.60	1551.00	1554.70
0.999	1470.69	1487.41	1499.41	1512.89	1524.37	1542.17	1554.34	1561.35	1563.20
0.996	1504.00	1518.27	1527.95	1539.17	1548.69	1563.20	1572.29	1576.48	1575.64
0.992	1553.18	1561.56	1565.95	1572.55	1577.88	1585.33	1589.23	1589.45	1585.52
0.983	1594.52	1597.40	1597.29	1600.04	1601.90	1603.15	1600.95	1596.62	1588.32
0.963	1645.05	1642.64	1637.06	1634.32	1630.80	1621.87	1610.94	1597.96	1582.61
0.934	1689.10	1679.72	1667.63	1658.81	1649.67	1630.76	1611.38	1590.99	1569.30
0.858	1692.68	1678.46	1661.79	1648.70	1635.49	1609.27	1583.53	1557.86	1531.67
0.804	1667.62	1652.83	1634.64	1620.69	1606.80	1579.37	1552.72	1526.32	1499.78
0.625	1633.87	1618.07	1599.37	1585.07	1570.94	1543.27	1516.67	1490.56	1464.43
0.426	1617.19	1600.46	1579.38	1564.34	1549.64	1521.58	1494.74	1468.63	1442.64
0.228	1611.57	1592.74	1571.42	1555.14	1539.75	1510.17	1481.82	1456.49	1430.06
0.000[d]	1603.78	1585.70	1564.28	1548.44	1533.25	1504.17	1476.43	1450.60	1424.41

[a] Expanded global uncertainty, U (c) = 1.0 m·s^{-1}, at a 95 % confidence level (k = 2)
[b] Standard uncertainty, $u(T)$ = 0.01 K$u(P)$ = 0.002 MPa
[c] Relative combined standard uncertainty, $u_{r,c}(x_w)$ = 0.002; [d] Extrapolated water-free value.

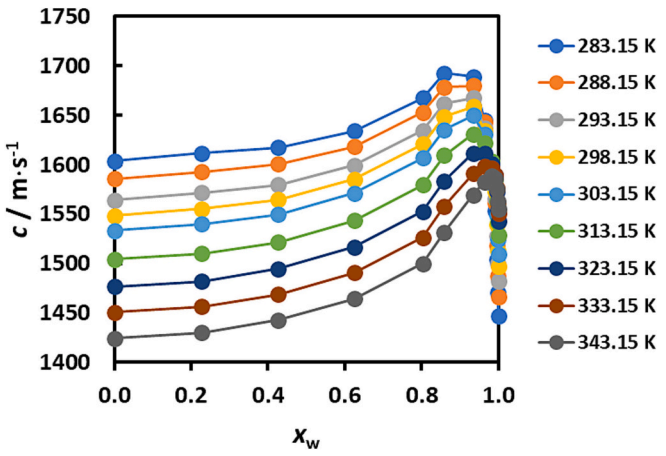

Fig. 4. Speed of sound, c, for the aqueous $[C_2mim][C_7H_{15}COO]$ system, at the studied temperatures, as a function of x_w.

maximum is displayed at lower values.

The water-free values for the speed of sound of $[C_2mim][C_7H_{15}COO]$ were obtained by fitting the four experimental values of the mass fraction of the ionic liquid, w_{IL}, closer to 1, as a linear function of the mass fraction of the ionic liquid, for each temperature, and then by extrapolating to $w_{IL} = 1$. The extrapolated water-free values of the speed of sound of the ionic liquid are also presented in the last line of Table 7 and Fig. 4. The water-free data can be correlated by Eq. (6):

$$c_{wf}\left(\mathrm{m} \bullet \mathrm{s}^{-1}\right) = a_1 + a_2 \times (T/\mathrm{K}) + a_3 \times (T/\mathrm{K})^2 \quad (6)$$

with coefficients $a_1 = (3605.7 \pm 188.6)$ m·s^{-1}, $a_2 = (-10.48 \pm 1.21)$ m·s^{-1}·K^{-1} and $a_3 = (0.0121 \pm 0.0019)$ m·s^{-1}· K^{-2}. The standard deviation was found to be 1.85 m·s^{-1}, with no point deviating by more than 2.6 m·s^{-1}.

Knowing the variation of the density and the speed of sound as a function of the composition, for a given temperature, it is possible to calculate the isentropic compressibility, κ_S, using Eq. 7. The values can be found in Table 8 and displayed in Fig. 5, where it can be seen that isentropic compressibility decreases slightly as the mole fraction increases, showing the same behaviour for the studied temperatures until $x_w \approx 0.98$. After this concentration, the isentropic compressibility increases sharply as it reaches the values of pure water, and an inversion of the temperature coefficient occurs, again suggesting a change in the structure of the mixture.

$$\kappa_S(Tx) = \frac{1}{\rho(Tx)\, c(Tx)^2} \quad (7)$$

The concept of intermolecular free lengths was introduced by Jacobson in 1951 [39] and further developed by himself and co-workers [40] to study the dependence of several thermodynamic and surface properties on the intermolecular forces in the liquid state. This concept is very interesting and has been applied to pure molecular solvents and ionic liquid systems. The definition of the intermolecular free length L_f is:

$$L_f = C_J \sqrt{\kappa_S} \quad (8)$$

Where κ_S is the isentropic compressibility and C_J is the Jacobsen constant, with a temperature variation proposed by Srinivasa Reddy et al. (2016) [41] and recently applied in [42], given by

$10^8 C_J = 93.87576 + 0.3757\ (T/\mathrm{K})$. Using the values of the isentropic compressibility reported in Table 8, it was possible to calculate the intermolecular free lengths for the pure ionic liquid and water, as well as their mixtures. These are shown in Table 9 and Figs. 6 and 7, as a function of temperature and composition.

This variation with temperature for the pure ionic liquid is much higher than for water, contributing to the inversion of the temperature dependence in the compressibility for water-rich mixtures.

These figures show that the variation L_f with the mole fraction of water is structured, starting to be smoothly decreasing with the increase in water mole fraction. Still, near a mole fraction $x_w \approx 0.8$, a change in slope occurs, passing through a minimum, changing to positive in the water-rich mixtures, as found for the isentropic compressibility. However, here there is no inversion of the temperature slope. Nevertheless, the change in the structure of the mixture is also noticed for $x_w > 0.95$. The temperature dependence found for the ionic liquid and water is shown in Fig. 7, and it can be seen that it increases linearly with temperature for the ionic liquid, while it is almost constant with a very weak negative slope up to 310 K, passing through a minimum, and then starting to increase with temperature for water. These results support the expansion of the structure of the ionic liquid with temperature, creating a loosely packed structure of the available molecules in the system (more thermal energy, greater free length), and the convergence of the curves L_f (x_w, T) in the mole fraction domain, when pure water is approached and the weak electrolyte structure starts to be dominant.

The deviation between the mixture intermolecular free lengths, $L_{f,mix}$, and the molar average of the pure components, ΔL_f, can be calculated with Eq. (9):

Table 8
Isentropic compressibility[a], κ_S, of the aqueous system $[C_2mim][C_7H_{15}COO]$ from $T = (283.15$ to $343.15)$ K[b], at $P = 0.1$ MPa[b], as a function of the mole fraction of water, x_w.

x_w[c]	$10^{10}\ \kappa_S$/ Pa^{-1}								
	283.15 K	288.15 K	293.15 K	298.15 K	303.15 K	313.15 K	323.15 K	333.15 K	343.15 K
1.000	4.776	4.658	4.559	4.477	4.409	4.312	4.253	4.228	4.231
0.999	4.620	4.520	4.452	4.378	4.319	4.235	4.187	4.171	4.184
0.996	4.410	4.331	4.281	4.224	4.179	4.118	4.089	4.088	4.116
0.992	4.122	4.083	4.066	4.038	4.019	3.998	3.998	4.019	4.063
0.983	3.895	3.888	3.896	3.891	3.891	3.903	3.935	3.979	4.046
0.963	3.642	3.661	3.695	3.717	3.743	3.805	3.879	3.967	4.072
0.934	3.438	3.486	3.547	3.595	3.646	3.754	3.869	3.996	4.135
0.858	3.406	3.475	3.557	3.625	3.696	3.843	3.996	4.157	4.331
0.804	3.511	3.585	3.678	3.753	3.831	3.991	4.157	4.332	4.517
0.625	3.674	3.758	3.858	3.941	4.025	4.197	4.373	4.557	4.753
0.426	3.770	3.861	3.980	4.069	4.159	4.341	4.526	4.718	4.921
0.228	3.811	3.914	4.036	4.135	4.231	4.427	4.626	4.818	5.030
0.000[d]	3.865	3.966	4.093	4.193	4.290	4.487	4.687	4.886	5.100

[a] Expanded global uncertainty, $U(K_s) = 0.01 \times 10^{10}$ Pa^{-1}, at a 95 % confidence level ($k = 2$)
[b] Standard uncertainty, $u(T) = 0.01$ K, $u(P) = 0.002$ MPa
[c] Relative combined standard uncertainty, $u_{r,c}(x_w) = 0.002$
[d] Extrapolated water-free value.

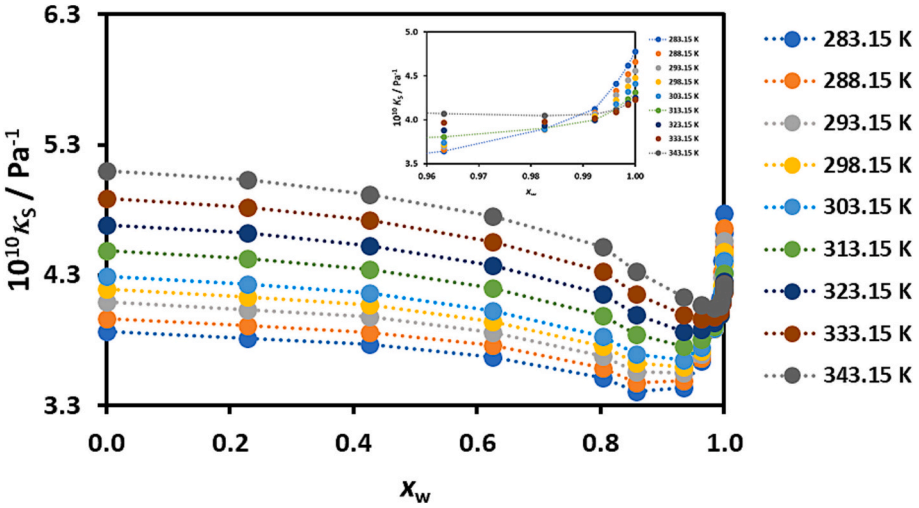

Fig. 5. Isentropic compressibility, κ_S, for the aqueous [C_2mim][C_7H_{15}COO] system, at the studied temperatures, as a function of x_w. The inset shows the inversion of the variation with temperature near the water-rich mixtures.

Table 9
Intermolecular free lengths, L_f[a], for the aqueous system [C_2mim][C_7H_{15}COO] from T = (283.15 to 343.15) K[b], at P = 0.1 MPa[b], as a function of the mole fraction of water, x_w.

x_w[c]	10^{10} L_f/ m								
	283.15 K	288.15 K	293.15 K	298.15 K	303.15 K	313.15 K	323.15 K	333.15 K	343.15 K
1.000	0.438	0.436	0.436	0.436	0.436	0.439	0.444	0.450	0.458
0.999	0.430	0.430	0.430	0.431	0.432	0.435	0.441	0.447	0.456
0.996	0.421	0.421	0.422	0.423	0.425	0.429	0.435	0.443	0.452
0.992	0.407	0.408	0.411	0.414	0.417	0.423	0.430	0.439	0.449
0.983	0.395	0.399	0.403	0.406	0.410	0.418	0.427	0.437	0.448
0.963	0.382	0.387	0.392	0.397	0.402	0.413	0.424	0.436	0.450
0.934	0.371	0.377	0.384	0.390	0.397	0.410	0.423	0.438	0.453
0.858	0.370	0.377	0.385	0.392	0.399	0.415	0.430	0.447	0.464
0.804	0.375	0.383	0.391	0.399	0.407	0.423	0.439	0.456	0.474
0.625	0.384	0.392	0.401	0.409	0.417	0.433	0.450	0.468	0.486
0.426	0.389	0.397	0.407	0.415	0.424	0.441	0.458	0.476	0.494
0.228	0.391	0.400	0.410	0.419	0.427	0.445	0.463	0.481	0.500
0.000	0.394	0.403	0.413	0.422	0.430	0.448	0.466	0.484	0.503

[a] Relative expanded global uncertainty, U_r (L_f) = 0.02, at a 95 % confidence level (k = 2)
[b] Standard uncertainty, $u(T)$ = 0.01 K, $u(P)$ = 0.002 MPa
[c] Relative combined standard uncertainty, $u_{r,c}(x_w)$ = 0.002.

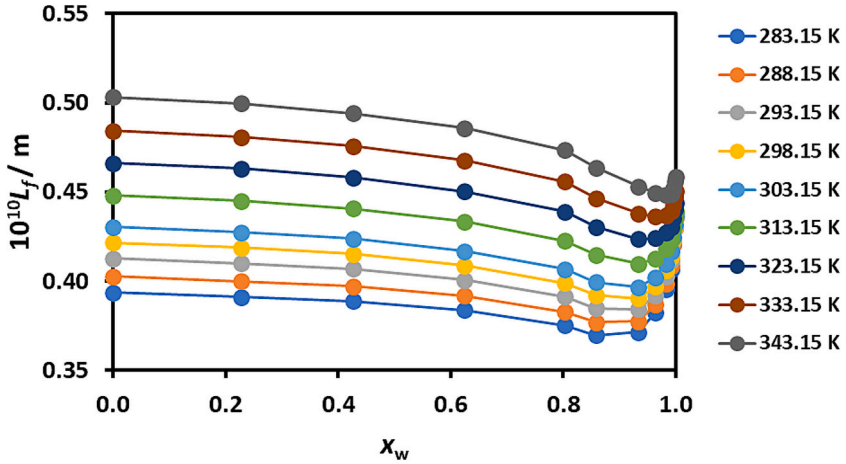

Fig. 6. Intermolecular free length, L_f, for the aqueous [C_2mim][C_7H_{15}COO] system, at the studied temperatures, as a function of x_w.

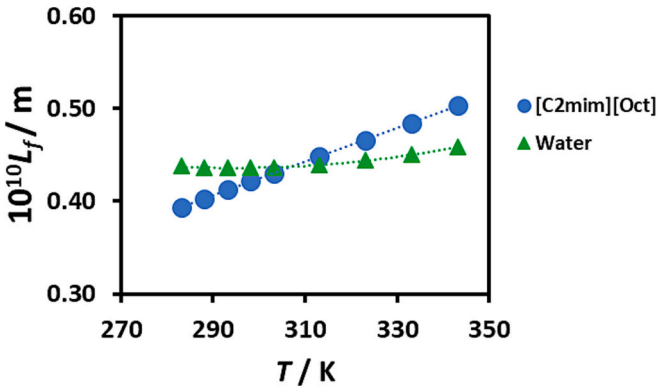

Fig. 7. Intermolecular free length, L_f, for the pure components, [C_2mim][C_7H_{15}COO] and water, at the studied temperatures.

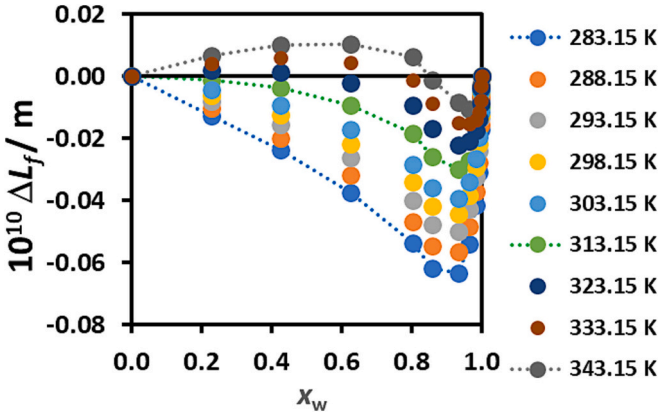

Fig. 8. Intermolecular free length deviation function, ΔL_f, for the aqueous [C_2mim][C_7H_{15}COO] system, at the studied temperatures, as a function of x_w. The dashed trend lines are drawn just to see the tendencies.

$$\Delta L_f = L_{f,mix} - \left(x_{IL}L^*_{f,IL} + x_W L^*_{f,W}\right) \tag{9}$$

where the asterisk represents the values for the pure components, at the same temperature and pressure as the mixture. Fig. 8 shows the results obtained.

This figure is very interesting, as it shows clearly the mixture behaviour and its temperature dependence. In addition, for the highest three temperatures, the variation is sigmoid, being positive at low mole fractions and negative at high mole fractions of water. This signifies a change in the intermolecular forces and the ease of movement of the molecules, namely the ionic liquid cation and anion, or clusters, and the balance of attractive and repulsive interactions (greater at higher temperatures.

Some authors consider that Eq. (9) defines an excess function, in the sense of the Gibbsian properties. A recent work [43] clarifies that L_f^E is not the same as our deviation function, by defining a new formula for the intermolecular free length in thermodynamic ideal mixtures, additive in a new "internal surface fraction" concentration scale. We intend to pursue this idea for ionic liquids aqueous mixtures, as the estimation method for the zero-temperature molar volume based on the critical temperature of the chemical compound cannot be used for these fluids.

Finally, as it is common to say that the shape of ΔL_f is similar to that of the excess volume, V^E, this is not the case for this system, as Figs. 3 and 8 show.

3.3. Thermal conductivity

The thermal conductivity is one of the most difficult properties to be measured with accuracy [24]. After the validation of the method as described above, 5 experimental measurements were obtained for each power input and cell temperature. There are no sets of available data in the literature for the thermal conductivity of either "pure" [C_2mim][C_7H_{15}COO] or of its mixtures with water to compare with.

The most extensive set of measurements for the thermal conductivity of [C_2mim][C_7H_{15}COO] was taken with the "pure" ionic liquid, as shown in Table 9, and having a water content (19,927 ± 313 ppm), a total of 88 data points. These were grouped into 16 average reference temperatures, T_{ref}. Table 10 shows the values for batches of 5 points, and the corresponding values of the averaged thermal conductivity, λ_{ref}, with the root mean square deviations. The results obtained are displayed in Fig. 9, along with the root mean square deviation of each thermal conductivity value. Eq. 10 is a linear fit with the coefficients

a_1 = (0.1733 ± 0.0014) W·m^{-1}·K^{-1}, a_2 = (7.93 × 10^{-6} ± 4.49 × 10^{-6}) W·m^{-1}·K^{-2}. The standard deviation of the fit is 0.0003 W·m^{-1}·K^{-1} (0.2 %), and no point deviates by more than 0.0006 W·m^{-1}·K^{-1}. The Figure shows that the thermal conductivity increases slightly with temperature, as found for other ionic liquids measured in this laboratory [3,16–18,25,26].

$$\lambda\left(\mathrm{W \bullet m^{-1} \bullet s^{-1}}\right) = a_1 + a_2 \times (T/\mathrm{K}) \tag{10}$$

As each experimental value has its reference temperature, T_{ref}, the data were grouped at nominal temperatures, T_{nom}, by using Taylor series expansion (Eq. 11), restricted to the linear variation as the dependence of the thermal conductivity on temperature is very small and the difference in temperatures seldom exceeds 2 K.

$$\lambda(T_{nom}) = \lambda\left(T_{ref}\right) + \left(\frac{\partial\lambda}{\partial T}\right)_{T_{ref}}\left(T_{nom} - T_{ref}\right) \tag{11}$$

The value of $\left(\frac{\partial\lambda}{\partial T}\right)$ was estimated for the mixture, considering the contributions from both the ionic liquid and the water, using Eq. 12:

$$\left(\frac{\partial\lambda}{\partial T}\right)_{T_{ref}} = x_w\left(\frac{\partial\lambda_w}{\partial T}\right)_{T_{ref}} + x_{IL}\left(\frac{\partial\lambda_{IL}}{\partial T}\right)_{T_{ref}} \tag{12}$$

where $\frac{\partial\lambda_w}{\partial T}$ was obtained from IUPAC SRD correlation [23], and $\frac{\partial\lambda_{IL}}{\partial T}$ was obtained by the linear regression of the sample experimental values of λ

Table 10
The thermal conductivity of "pure" [C_2mim][C_7H_{15}COO][a] (w_w = 0.0199, x_w = 0.2814), from
T = (290.72 to 352.81) K[b], at P = 0.1 MPa[b], as a function of temperature.

T_{ref} / K	σ / K	λ_{ref} / W·m^{-1}·K^{-1}	σ_λ / W·m^{-1}·K^{-1}
290.72	0.03	0.1757	0.0003
292.28	0.29	0.1753	0.0006
295.70	0.09	0.1756	0.0003
297.82	0.11	0.1756	0.0007
300.77	0.03	0.1759	0.0002
301.29	0.20	0.1758	0.0005
305.17	0.45	0.1755	0.0002
307.41	0.15	0.1753	0.0005
311.70	0.38	0.1759	0.0002
318.13	0.18	0.1760	0.0008
321.53	0.40	0.1765	0.0004
328.74	0.27	0.1755	0.0006
331.78	0.42	0.1765	0.0007
339.04	0.07	0.1757	0.0004
349.73	0.03	0.1757	0.0004
352.81	0.22	0.1762	0.0011

[a] Expanded relative global uncertainty, U_r (λ) = 0.02 W·m^{-1}·K^{-1}, at a 95 % confidence level (k = 2);
[b] Standard uncertainty, $u(T)$ = 0.01 K, $u(P)$ = 0.002 MPa.

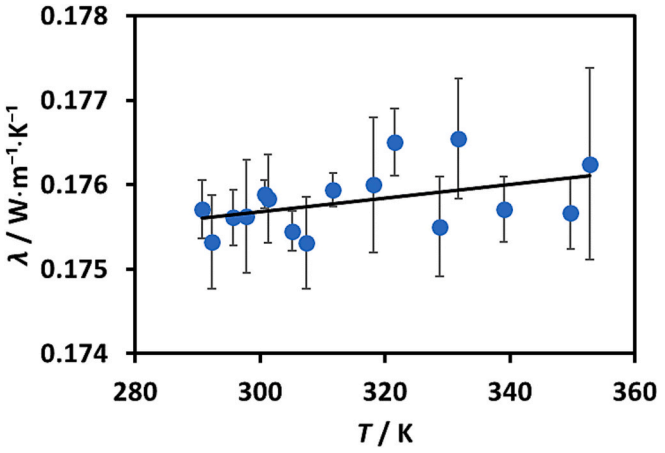

Fig. 9. The thermal conductivity of "pure" [C_2mim][C_7H_{15}COO] ($w_w = 0.0199$, $x_w = 0.2814$), showing the root mean square deviation bar for each experimental averaged point. The straight line reproduces Eq. 10.

with lower water content (19,927 ± 313 ppm), Eq. 10. The experimental data, corrected for the same nominal temperatures, are presented in Table 11 and Fig. 10.

To obtain water-free values, a linear regression of the experimental values the sample with lower water content was performed, and the experimental values for this concentration were corrected for each nominal temperature. After that, the four experimental values closer to $w_w = 0$ were fitted as a linear function of the mass fraction of the ionic liquid, for each nominal temperature. The water-free values were then obtained using Eq. 13 to extrapolate the value from the last measured mass fraction

($w_w = 0.0199$) to pure ionic liquid, water-free.

$$(\lambda_{wf})_T = (\lambda_T)_{w_w=0.0199} - 0.0199 \times \left(\frac{\partial \lambda}{\partial w_w}\right)_T \quad (13)$$

The water-free values of the thermal conductivity of the ionic liquid are also presented in the last line of Table 10 and are present in Fig. 10. Given the fact that the variation with temperature is almost zero, it can be assumed that the water-free thermal conductivity of the pure ionic liquid is temperature-independent. For the studied temperature range (288.15–348.15) K, an average value of

$\lambda_{wf} = 0.1695 \pm 0.0002$ W·m^{-1}·K^{-1} was obtained, consistent with the correlation of the raw experimental data. From the analysis of Fig. 10, thermal conductivity is found to be temperature independent up until $w_w \approx 0.90$ ($x_w \approx 0.61$), slowly increasing as the mole fraction increases. After that, the thermal conductivity increases as it approaches the thermal conductivity of pure water. The increase of thermal conductivity as a function of the mole fraction of water and temperature has been previously reported [44]. At $x_w \approx 0.998$, a possible maximum on thermal conductivity was found for the highest temperatures, having average values 5 % higher than those of the pure water (see insert in Fig. 10). This maximum is also present in other ionic liquid + water systems studied by our group [17,18] and can be particularly useful for heat transfer applications.

The thermal conductivity of the mixtures variation with temperature and composition can be correlated with quadratic functions of the type given by Eq. 14:

$$\lambda_{exp}(w_w, T) = \sum_{i=0}^{2} g_i(T) {w_w}^i \quad (14)$$

The coefficients are given in Table S3, with their standard deviations and the standard deviation of the fit, for each temperature. Deviations of each experimental point from the fit can be seen in Fig. S3 and do not exceed ±2 %, except for 4 points for the mass fraction 0.2, which can reach 2.5 %. These deviations are commensurate with the claimed uncertainty of our experimental data, 2 %.

The data obtained can be used to calculate the deviation between the experimental thermal conductivity and the thermal conductivity calculated from the molar average of the individual contributions of the ionic liquid and the water, as given by Eq. 15, and the results can be seen in Fig. 11.

$$\Delta\lambda = \lambda_{mix} - x_w\lambda_w - x_{IL}\lambda_{IL} \quad (15)$$

As shown in Fig. 11, the deviations are negative in all composition range, except for very high-water mole fractions, where a temperature dependence inversion is also found. This fact can be justified by the presence of a maximum in thermal conductivity, as explained before, for the compositions near pure water, at higher temperatures. The values are almost temperature independent, and the minimum is obtained at about $x_w \approx 0.86$, the same composition where a maximum in density and speed of sound is found. These results may support the eventual existence of a change in the molecular structure of this aqueous system, as previously referred to.

It is interesting to understand the relation of the thermal conductivity of the pure ionic liquid with other liquid variables, trying to identify its dependence on molecular structure and molecular in-

Table 11
Thermal conductivity[a], λ, of the aqueous system [C_2mim][C_7H_{15}COO] from T = (288.15 to 348.15) K[b], at P = 0.1 MPa[b], as a function of the mole fraction of water, x_w.

x_w[c]	w_w	λ / W·m^{-1}·K^{-1}								
		288.15 K	293.15 K	298.15 K	303.15 K	308.15 K	318.15 K	328.15 K	338.15 K	348.15 K
1.0000	1.0000	0.5888	0.5936	0.5982	0.6003	0.6037	0.6121	0.6148	0.6215	0.6269
0.9986	0.9800	0.5916	0.5906	0.5974	0.6114	0.6206	0.6378	0.6461	0.6487	0.6729
0.9963	0.9500	0.5702	0.5788	0.5784	0.5846	0.5872	0.5981	0.5969	0.5845	0.6017
0.9922	0.9000	0.5472	0.5457	0.5531	0.5581	0.5526	0.5719	0.5770	0.5620	0.5877
0.9826	0.8000	0.4809	0.4848	0.4888	0.4873	0.4915	0.5170	0.5047	0.5127	0.5261
0.9633	0.6500	0.3998	0.4124	0.4092	0.4092	0.4124	0.4136	0.4207	0.4304	0.4324
0.9339	0.5000	0.3323	0.3324	0.3373	0.3374	0.3381	0.3448	0.3493	0.3509	0.3600
0.9040	0.4000	0.2898	0.2984	0.2938	0.2945	0.2963	0.3007	0.3020	0.3083	0.3102
0.8582	0.3000	0.2548	0.2582	0.2580	0.2577	0.2592	0.2605	0.2627	0.2658	0.2658
0.7606	0.1837	0.2241	0.2243	0.2256	0.2243	0.2253	0.2271	0.2279	0.2303	0.2328
0.6109	0.1001	0.1961	0.1957	0.1961	0.1963	0.1950	0.1981	0.1991	0.2006	0.2013
0.4265	0.0500	0.1837	0.1828	0.1821	0.1829	0.1833	0.1835	0.1837	0.1846	0.1863
0.2814	0.0199	0.1756	0.1751	0.1753	0.1756	0.1749	0.1757	0.1754	0.1760	0.1753
0.0000[d]	0.0000	0.1697	0.1697	0.1695	0.1698	0.1697	0.1695	0.1695	0.1693	0.1692

[a] Expanded global uncertainty, $U(\lambda) = 0.02$ W m^{-1} K^{-1}, at a 95 % confidence level ($k = 2$)
[b] Standard uncertainty, $u(T) = 0.02$ K, $u(P) = 0.002$ MPa
[c] Relative combined standard uncertainty, $u_{r,c}(x_w) = 0.002$
[d] Extrapolated water-free value.

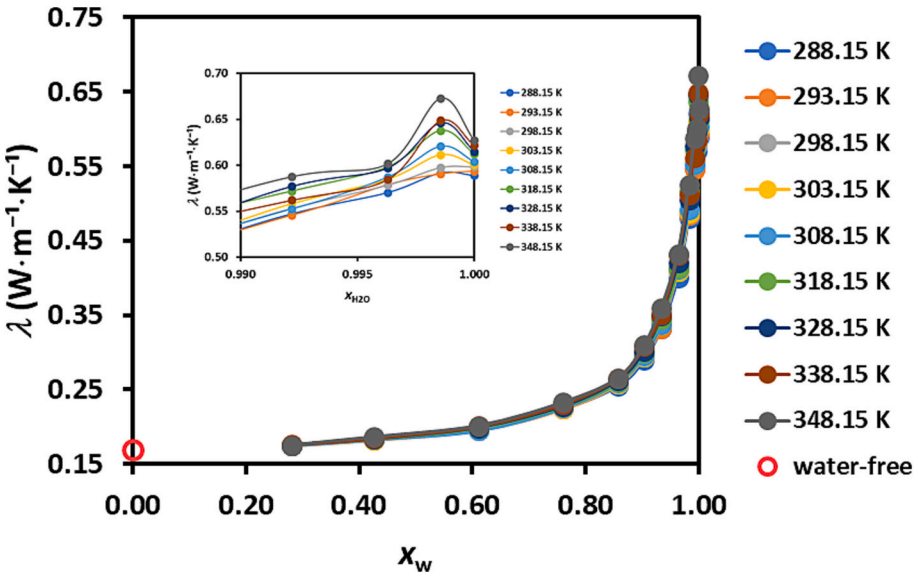

Fig. 10. Thermal conductivity, λ, for the aqueous [C_2mim][C_7H_{15}COO] system, at the studied temperatures, as a function of x_w. The inset shows the values for $x_w > 0.99$, where a maximum near 0.998 is found, increasing with temperature.

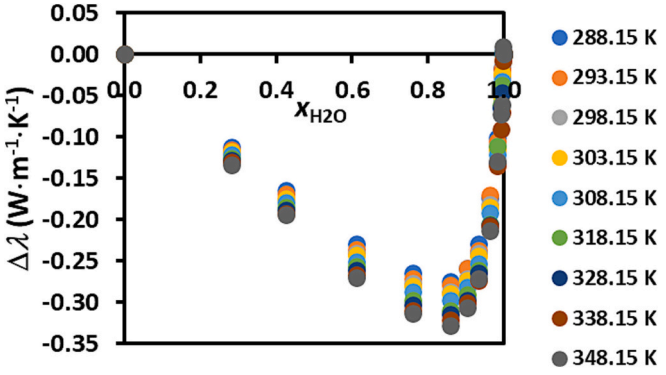

Fig. 11. Thermal conductivity deviations for the aqueous [C_2mim][C_7H_{15}COO] system, at the studied temperatures, as a function of the mole fraction of water.

teractions. This problem has been discussed recently in several of our publications [3,27,45], and the results obtained were very interesting. P. W. Bridgman, in his pioneer work, developed one of the most relevant theories to calculate the thermal conductivity of liquids [46]. Bridgman assumed a cubic arrangement of the molecules and related the molecular volume (v^*) and the speed of sound of a fluid, c, to obtain its thermal conductivity by Eq. 16:

$$\lambda = 2.8 k_B (v^*)^{-2/3} c \quad (16)$$

Where λ is the thermal conductivity of the liquid, and k_B is the Boltzmann constant. This equation is very simple, and when the density, ρ, and speed of sound, c, are known, the thermal conductivity of the ionic liquid is easily computed, as $v^* = M/(\rho\, N_0)$, N_0 being the Avogadro number.

As discussed in [3], the numerical coefficient was initially 3 but was empirically modified to 2.8 to secure better agreement with experimental data for molecular and associated liquids, although it has been questioned by several authors [47–49]. This theory, when applied with values of density and speed of sound obtained in this work, produced values almost 80 % inferior to the experimental ones, has it can be seen in Table 11.

In a recent paper from our group [45], we have discussed the possibility of obtaining the value of this numerical coefficient, designated by *K*, and found that for It is clear that the constant has a linear variation with temperature, varying between $6 < K < 5.68$, much higher than 2.8. For [C_2mim][C_7H_{15}COO], we found the values reported in the last row of Table 12, also varying with temperature, $4.36 < K < 5.00$, confirming the previous tendency. In this paper, an empirical relation with the molecular mass, *M*, at 303.15 K was also proposed, that can lead to a new estimation method for the ionic liquids' thermal conductivity in the future. This *easy-to-use* empirical relation is given by Eq. 17:

$$\lambda_{T=303.15\ K}\left(\mathrm{W \bullet m^{-1} \bullet K^{-1}}\right) = 2.609 \times M\left(\mathrm{g{\cdot}mol^{-1}}\right)^{-0.5} \quad (17)$$

This equation, although very simple, reduced the deviation from about 62 % to 3.8 %, which proves that the relation between the negative square root of the molecular mass and the thermal conductivity could be useful in future theories to estimate the thermal conductivity of ionic liquids and even other fluids.

Table 12
Comparison between the thermal conductivity for [C_2mim][C_7H_{15}COO], λ, obtained by the Bridgman Theory using values of density[a] and speed of sound[b] obtained in this work, and the experimental values, from $T = (288.15$ to $348.15)$ K[c].

	288.15 K	293.15 K	298.15 K	303.15 K	308.15 K	318.15 K	328.15 K	338.15 K	348.15 K
c / m·s^{-1}	1584.31	1566.90	1550.09	1533.88	1518.28	1488.88	1461.88	1437.30	1415.13
ρ / kg·m^{-3}	1002.34	998.72	995.17	991.69	988.29	981.71	975.43	969.44	963.74
λ / W· m^{-1}·K^{-1}	0.109	0.107	0.106	0.105	0.103	0.101	0.099	0.097	0.095
Deviation / %	−55.81	−57.90	−59.84	−62.15	−64.14	−67.96	−71.77	−75.24	−78.54
K	4.36	4.42	4.48	4.54	4.60	4.70	4.81	4.91	5.00

[a] Standard uncertainty, $U(\rho) = 0.27$ kg m^{-3}
[b] Standard uncertainty, $u(c) = 1.85$ K
[c] Standard uncertainty, $u(T) = 0.02$ K.

The problem is more complex for mixtures. The presence of unlike interactions between the ionic liquid and water plays a significant role, as they can be very different from the pure component interactions, as already known from previous studies [13,17,18]. Unlike molecular interactions originate additional thermal resistances to heat conduction, that are dependent on the composition, for a given temperature.

The Filaments Model, introduced by Melkikh and Skripov in 2023 [50], admits that the dependence on concentration of the thermal conductivity of liquid mixtures arises from different thermal resistances, connected in series, the pure component thermal conductivities, λ_1^* and λ_2^*, the mass fractions of the components in the mixtures, w_1 and $w_2 = 1 - w_1$, and a parameter γ, dependent on the mass ratio of the two components, m_1 and m_2. In this model, the thermal conductivity of the mixture, λ, is given by Eq. 16:

$$\lambda = \frac{\lambda_1 \lambda_2}{w_1 \lambda_2 + (1 - w_1)\lambda_1} \tag{18}$$

where λ_1 and λ_2 are the values of the pure components, corrected by the presence of the other component (in essence correcting the interactions/thermal resistances by the presence of the different component of the mixture), given by Eq. 19:

$$\lambda_1 = \lambda_1^*[w_1 + (1 - w_1)\gamma]$$

$$\lambda_2 = \lambda_2^*[(1 - w_1) + w_1\gamma] \tag{19}$$

The Bridgman model was used to calculate the parameter γ to account for the phonon scattering by the different types of molecules present in the mixture. The authors calculated γ by Eq. 20, as a function of the mass ratio between the two components, m_2/m_1:

$$\gamma = 1 - \frac{\left(\sqrt{\frac{m_2}{m_1}} - 1\right)^2}{\left(\sqrt{\frac{m_2}{m_1}} + 1\right)^2} \tag{20}$$

In a previous paper [18], we reported the application of the Filaments model to estimate the thermal conductivity of the binary mixture of the system [C_2mim[[N(CN)$_2$] + water. The results obtained show that the model underestimates the thermal conductivity of the mixtures by a large factor in the entire temperature range, namely for $0.2 < w_w < 0.9$. For the system here reported, the obtained results are shown in Fig. 12, also for the extreme temperatures (other temperatures not displayed for clarity). It is clear that, also for this system, the Filaments Model underestimates the value of the thermal conductivity of the [C_2mim][C_7H_{15}COO] aqueous system, the result being almost temperature independent.

To get a more complete picture of this behaviour for these and other aqueous studied systems, with different ionic liquids, like [C_2mim][CH_3COO] [13] and [C_2mim][CH_3SO_3] [17], we have calculated, at 293.15 K the deviation function $\Delta = \lambda_{exp} - \lambda_{Fil}$, as a function of the mass fraction of water, w_w of all four systems. The quantities necessary for the calculation are displayed in Table 13, designating water as component 1, and the results obtained are shown in Fig. 13.

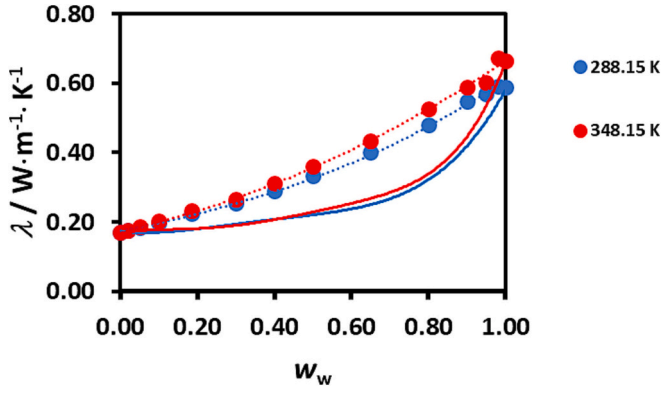

Fig. 12. Comparison between the experimental results (dots) and the Filaments Model (lines) for the extreme temperatures, 288.15 K and 348.15 K.

Table 13
Parameters used for the calculation of the thermal conductivity of the binary systems.

	M / g·mol^{-1}	γ	$\sqrt{(m_2/m_1)}$
[C_2mim[[N(CN)$_2$]	177.21	0.7332	3.1364
[C_2mim][CH_3SO_3]	206.26	0.7043	3.3837
[C_2mim][CH_3COO]	170.21	0.7409	3.0738
[C_2mim][C_7H_{15}COO]	254.37	0.6640	3.7576
H_2O	18.015	–	–

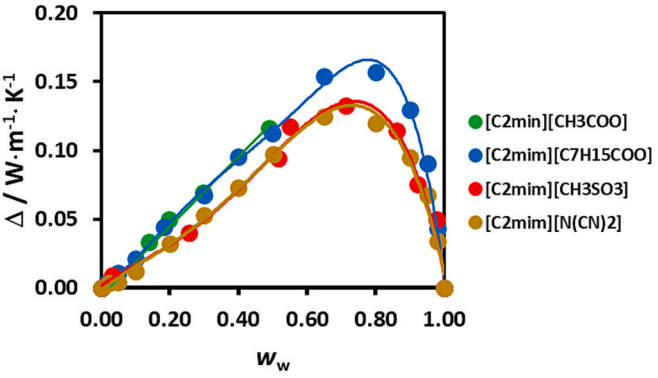

Fig. 13. The deviation function Δ as a function of the mass fraction of water, w_w, for all systems studied, at $T = 293.15$ K, except for [C_2mim[[N(CN)$_2$] + water. The lines are just trend lines to better show the differences.

From this Fig. 13, we can conclude: First, the deviation Δ is very significant for all the systems, being of the order of 0.12 to 0.16 W·m^{-1}·K^{-1} in the maximum, obtained for $0.7 < w_w < 0.8$, $0.96 < x_w < 0.98$, and very close to pure water. Secondly, two pairs appear with the same variation; The higher deviations for [C_2mim][CH_3COO] and [C_2mim][C_7H_{15}COO], and the lowest rim for [C_2mim[[N(CN)$_2$] and [C_2mim][CH_3SO_3]. Thirdly, the different values and mass ratios present in Table 12 cannot explain this behaviour. The data for [C_2mim][CH_3COO] does not cover the highest mass fractions of water. Nevertheless, the fair agreement for all different anions in the lowest mass fractions is interesting, as the anions are extremely different in size and mass. The Filaments models' authors suggested that other effects must be considered, namely average distances between molecules and strengths of chemical bonds [50]. However, due to the specific behaviour of the IL + water mixtures, we suggest that the difference between the sizes of molecules and the structure (packing, clusters, strings of water molecules) is the most probable driver to correct the Filaments Model.

3.4. Refractive index

The measured values for the refractive index for the system [C_2mim][C_7H_{15}COO] + water are all shown in Table 14 and displayed in Fig. 14. The values for the "pure" ionic liquid were corrected to water-free values, also presented in Table 14, by fitting the three values closer to $x_w = 0$ at each measuring temperature, and extrapolating them linearly for $x_w = 0$.

The water-free values were fitted to a polynomial Eq. 21:

$$n^D = h_0 + h_1 T(\mathrm{K}) + h_2 T(\mathrm{K})^2 \tag{21}$$

With a standard deviation of 0.0007, at a 95 % confidence level ($k =$

Table 14
Refractive index (sodium D line)[a], n^D, for $[C_2mim][C_7H_{15}COO]$ + water mixtures, from T = (283.15 to 343.15) K[b], at P = 0.1 MPa[b], as a function of the mole fraction of water.

x_w[c]	n^D								
	283.15 K	288.15 K	293.15 K	298.15 K	303.15 K	313.15 K	323.15 K	333.15 K	343.15 K
1.0000	1.33397	1.33398	1.33321	1.33270	1.33212	1.33076	1.32916	1.32736	1.32543
0.9980	1.33796	1.33759	1.33712	1.33657	1.33595	1.33452	1.33287	1.33102	1.32897
0.9960	1.34321	1.34276	1.34223	1.34162	1.34095	1.33941	1.33766	1.33571	1.33358
0.9929	1.34970	1.34914	1.34850	1.34780	1.34532	1.34537	1.34349	1.34145	1.33925
0.9827	1.36784	1.36702	1.36614	1.36521	1.36417	1.36210	1.35962	1.35726	1.35481
0.9624	1.39241	1.39133	1.39022	1.38911	1.38798	1.38561	1.38314	1.38049	1.37773
0.9331	1.41586	1.41460	1.41333	1.41204	1.41075	1.40807	1.40532	1.40251	1.39968
0.9045	1.43089	1.42951	1.42810	1.42671	1.42529	1.42243	1.41952	1.41655	1.41354
0.8579	1.44513	1.44367	1.44219	1.44071	1.43923	1.43623	1.43319	1.43009	1.42697
0.7842	1.46082	1.45931	1.45781	1.45631	1.45482	1.45188	1.44887	1.44585	1.44292
0.6152	1.47356	1.47205	1.47053	1.46903	1.46753	1.46453	1.46160	1.45880	1.45637
0.4160	1.47866	1.47716	1.47566	1.47417	1.47273	1.46980	1.46691	1.46412	1.46142
0.1026	1.48675	1.48520	1.48365	1.48212	1.48060	1.47759	1.47463	1.47172	1.46897
1.0000[d]	1.48939	1.48783	1.48629	1.48475	1.48325	1.48025	1.47729	1.47438	1.47153

[a] Expanded global uncertainty, $U(n^D) = 0.0002$, at a 95 % confidence level ($k = 2$)
[b] Standard uncertainty, $u(T) = 0.03$ K, $u(P) = 0.002$ MPa
[c] Relative combined standard uncertainty, $u_{r,c}(x_w) = 0.002$
[d] Extrapolated water-free value.

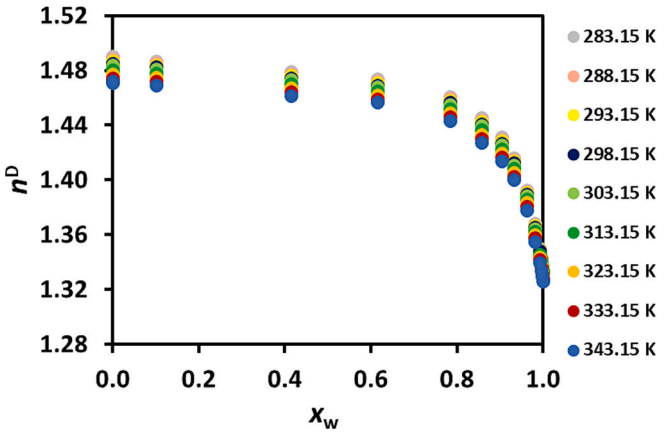

Fig. 14. The variation of the refractive index of the aqueous $[C_2mim][C_7H_{15}COO]$ system, as a function of the mole fraction of water, at the different temperatures.

2). No data deviates from the line by more than 0.00001. The coefficients and their standard deviations are $h_0 = 1.59626 \pm 0.00071$, $h_1 = -4.433 \times 10^{-4} \pm 0.046 \times 10^{-4}$ and $h_2 = 2.326 \times 10^{-7} \pm 0.073 \times 10^{-7}$. The values obtained at each temperature are also shown in Fig. 14. This Figure shows that the refractive index has a monotonic variation with the molar fraction of water in the mixture and that the temperature dependence is small.

There are no sets of available data in the literature for the refractive index of either "pure" $[C_2mim][C_7H_{15}COO]$ or of its mixtures with water to compare with.

The refractive index of an ideal solution can be calculated by Eq. 22 [51]:

$$n^{D\,id}(\varphi, T, P) = \left(\varphi_w n_w^{D^2} + \varphi_{IL} n_{IL}^{D^2}\right)^{1/2} \quad (22)$$

where φ_i are the volume fractions of component i (w, IL). From that, it is possible to calculate the excess refractive index given by Eq. 23. For these calculations, density values obtained in this work were used. The values of the excess refractive index are shown in Table S4 and displayed in Fig. 15. It is possible to see that, except for the region near $\varphi_w = 0$, the excess refractive index is within the uncertainty of the calculation (±

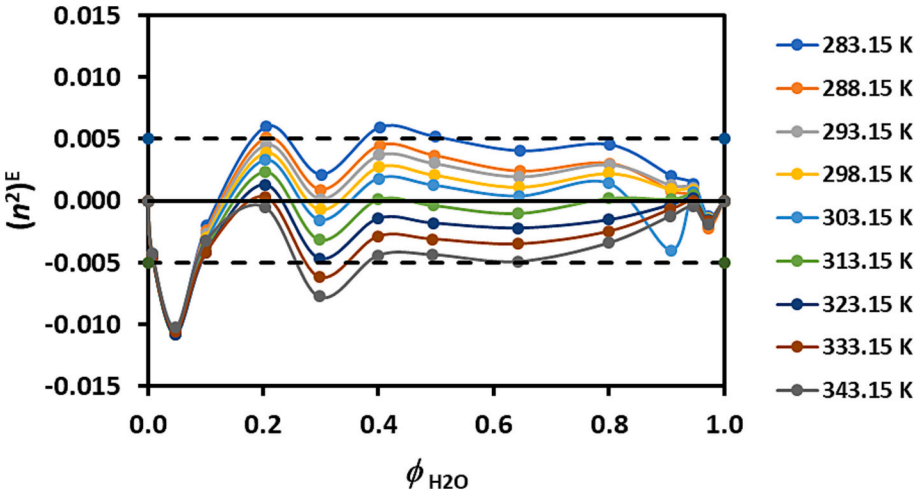

Fig. 15. The variation of the excess refractive index of the aqueous $[C_2mim][C_7H_{15}COO]$ system, as a function of the volume fraction of water, at the different temperatures. The dashed line represents the standard uncertainty of the excess refractive index calculation, $u((n^2)^E) = 0.005$.

0.005 at 95 % confidence level), and therefore the mixture can be considered as "ideal" for this optical property.

$$\left(n^{D^2}\right)^E = n^{D^2}{}_{mix}(\varphi,T,P) - \left(n^{D\,id}(\varphi,T,P)\right)^2 = n^{D^2}{}_{mix}(\varphi,T,P) - \left(\varphi_w n^{D^2}{}_w + \varphi_{IL} n^{D^2}{}_{IL}\right) \quad (23)$$

Another property that can be derived from the density and refractive index data is the excess molar refraction, defined by Eq. 24 [52]. The values are shown in Table S4 and Fig. 16, where it can be seen that this property has a parabolic shape variation (4th grade) with the mole fraction of water, with a minimum at $x_w \approx 0.4$, and is weakly dependent on temperature. This minimum appears in a much smaller molar fraction of water compared with the excess volume minimum.

$$R^E = R_m - R_m^{id} = \left(\frac{n^{D^2}-1}{n^{D^2}+2}\right)V_m - \left(\frac{n^{D^{id^2}}-1}{n^{D^{id^2}}+2}\right)V_M^{id} \quad (24)$$

It will be interesting to demonstrate that the ideal molar refraction is additive. In the past, it has been assumed that this was indeed true for molecules of simple molecular constitution, which is not the case for an ionic liquid [53]. We can test its validity by plotting the similarity diagram of the two quantities, Y_1 and Y_2, with the different definitions of the molar refraction of an ideal solution, Eq. 25 and Eq. 26:

$$Y_1 = R_m^{id} = \left(\frac{n^{D^{id^2}}-1}{n^{D^{id^2}}+2}\right)V_M^{id} \quad (25)$$

and

$$Y_2 = R_m^{id} = x_{IL}R_{m,IL} + x_w R_{m,w} \quad (26)$$

The results obtained for the two extreme temperatures, 283.15 K and 343.15 K, are shown in Fig. 17.

The departure between Y_1 and Y_2 is never greater than 0.014 $cm^3 \cdot mol^{-1}$, which is well within the expanded global uncertainty of the molar refraction calculation based on the measured refractive indices. This result proves that the molar refraction is additive and almost temperature independent in the range studied. We hope to detail identical calculations for other aqueous ionic-liquid systems in order to support this conclusion.

3.5. Cytotoxicity in vitro against the HepG2 cell line

To evaluate human health risk and identify the safety profile of [C_2mim][C_7H_{15}COO], its cytotoxicity was assessed in vitro using human HepG2 liver cells. As the liver is the primary organ responsible for the metabolism and detoxification of xenobiotics and other chemical agents,

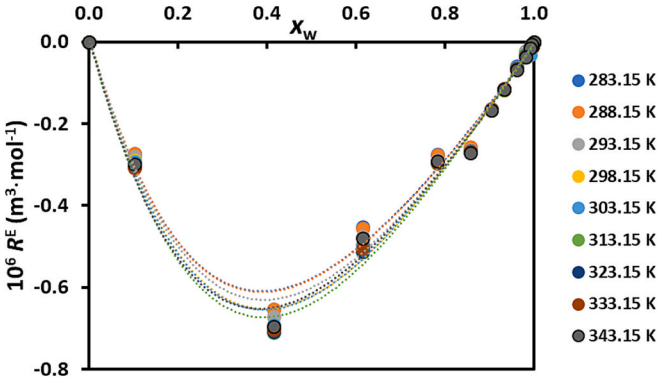

Fig. 16. The variation of the excess molar refraction of the aqueous [C_2mim][C_7H_{15}COO] system, as a function of the mole fraction of water, at the different temperatures. Dashed lines are trend lines to visualize the temperature dependence.

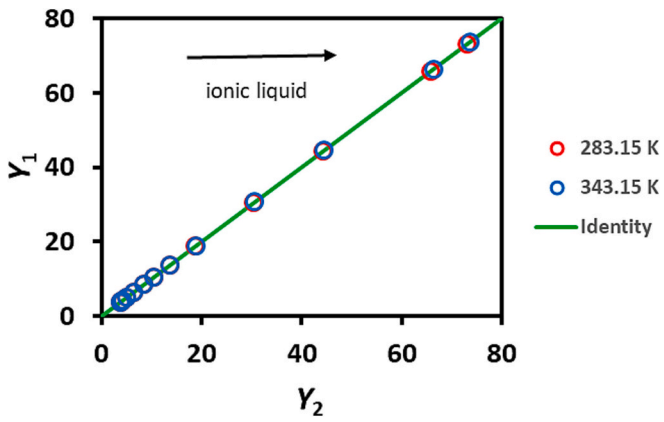

Fig. 17. Similarity plot for the two definitions of molar refraction of an ideal mixture, calculated for the system [C_2mim][C_7H_{15}COO] + H_2O. Only 2 temperatures are shown to keep clarity in the plot.

the HepG2 cell line was selected as a relevant model for assessing potential toxic effects of [C_2mim][C_7H_{15}COO] in humans. This human-derived hepatic cell line is widely used in toxicity evaluation due to chemical exposure, considering its metabolic activity and similarity to liver functions [54].

HepG2 cells were exposed for 24 h to different concentrations of [C_2mim][C_7H_{15}COO], between x and y, and cell viability was assessed using the MTT assay. A dose-response curve was generated by representing the percentage of cell death as a function of the logarithm of the [C_2mim][C_7H_{15}COO] concentrations tested (Fig. 18). The obtained sigmoidal dose-response curve demonstrated a clear concentration-dependent cytotoxic effect of [C_2mim][C_7H_{15}COO], with cell death increasing progressively from approximately 20 % to nearly 100 %, across the tested concentration range. A non-linear regression model was used for analysis, and the data were fitted to a sigmoidal Hill regression model using GraphPad Prism 5. The model showed a good fit, with an R^2 value of 0.9819, indicating a high consistency of the regression. From the fitted curve, both the LC_{50} value—the concentration at which 50 % of the cells were non-viable- and the Hill slope—reflecting the steepness of the response—were determined (Table 16).

The LC_{50} value obtained for [C_2mim][C_7H_{15}COO] in HepG2 cells was 9.2 mM (equivalent to 2333 mg·L^{-1}), indicating relatively low cytotoxicity. This value is higher than those reported for several other imidazolium-based ionic liquids, suggesting that with a higher value than LC50 values reported for other ILs, suggesting that [C_2mim][C_7H_{15}COO] may be less harmful than other studied ILs. Although

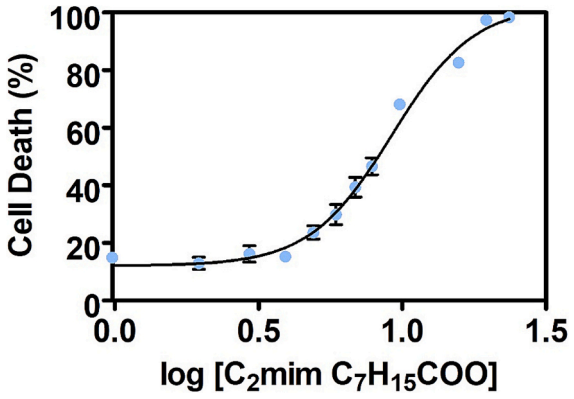

Fig. 18. Dose–response curve for [C_2mim][C_7H_{15}COO]-induced cytotoxicity in HepG2 cells after 24-h exposure. Values represent the mean ± standard deviation ($n = 6$).

Table 16
Parameters of [C_2mim][C_7H_{15}COO] in HepG2 cells obtained from non-linear regression analysis with the Hill equation (GraphPad Prism 5). Values represent the best-fit estimates with associated confidence intervals.

		C_2mim C_7H_{15}COO
LC_{50}	mg·L^{-1}	2,333 ± 178[a]
	M	0.0091 ± 0.0007[a]
	mM	9.2 ± 0.7[a]
HillSlope		3.0 ± 0.6 [a]
R^2		0.9819

[a] Confidence level of 95 %.

literature data on the cytotoxicity of ILs in human cell lines remains limited, Li et al. [55] reported an LC_{50} of 0.44 mM for [C_8mim][Br] in HepG2 cells after 24 h exposure, while Zhang et al. found LC_{50} values of 0.46 mM and 0.01 mM for [C_4mim][Cl] and [C_8mim][Cl], respectively, under similar conditions [56]. Compared to these, [C_2mim][C_7H_{15}COO] exhibits a significantly lower cytotoxic profile.

These differences are likely attributed to the structure of the ILs, particularly the alkyl chain length on the imidazolium cation. Both Zhang et al. [56] and Frade et al. [57] observed that increased alkyl chain length correlates with higher cytotoxicity. Given that [C_2mim][C_7H_{15}COO] contains a relatively short ethyl side chain on the cation, this structural feature may explain its reduced toxicity in comparison to [C_8mim]-based ILs.

This fact is described in the literature with other types of ILs in other cell lines, and could be the reason why the LC50 values determined in this work (in ILs with a smaller aliphatic chain in the cation) are higher than those mentioned previously. [58,59]. Moreover, environmental considerations may suggest a favorable profile for [C_2mim][C_7H_{15}COO]. Gonçalves et al. [8] referenced the toxicity classification scale by Passino and Smith [60], originally developed to evaluate aquatic toxicity in *Daphnia pulex*. According to this scale, chemicals with LC_{50} values above 1000 mg/L are classified as "relatively harmless." While the present study does not assess *Daphnia pulex* directly, the comparatively high LC_{50} value observed in HepG2 cells, alongside structural factors, suggests that [C_2mim][C_7H_{15}COO] may pose a lower environmental hazard than other ILs. Nevertheless, further ecotoxicological studies are required to confirm this inference.

4. Conclusions

The ionic liquid 1-Ethyl-3-methylimidazolium octanoate is an important chemical for new applications in the fiber industry, namely as an extractant and additive in process operations.

This paper reports on the first experimental data for density, speed of sound, thermal conductivity, and refractive index of this ionic liquid and its mixtures with water, in the full composition range, at

$P = 0.1$ MPa. Values for the "water-free" ionic liquid were calculated. Considering the potential applications of this IL as a green fluid, the present study provides a novel quantitative evaluation of [C_2mim][C_7H_{15}COO] cytotoxicity, supporting its classification as a relatively safer imidazolium-based IL. An LC_{50} value of 9.2 mM was determined in HepG2 liver cells, indicating lower cytotoxicity compared to other ILs with longer alkyl chains on the cation.

This mixture has some properties that have some similarity to systems previously studied [13,16,17], but some discussion is necessary. In the first place, the density of the pure liquid is very similar to that of water, varying between 966 and 1005 kg·m^{-3}, which suggests the same type of packaging in the liquid state, although molecular masses are very different, and therefore the molar volumes. The excess volumes are negative, suggesting an attractive interaction with water, as it was found for [C_2mim][CH_3COO] and [C_2mim][CH_3SO_3], but different than those for [C_2mim[[$N(CN)_2$], which were found to be positive, an indication of possible repulsion. Only data on excess enthalpy in this system, currently not available, can prove this assumption definitively. This result also supports better packaging for the mixture.

The thermal expansion coefficient variation with composition and temperature is similar to previous studies. The speed of sound and the isentropic compressibility show similar behaviour to the other mixtures, with the temperature inversion for the highly diluted aqueous solution, weak electrolyte zone. The evaluation of the Jacobsen intermolecular free length showed that its variation with temperature for the pure ionic liquid is much higher than for water, possibly contributing to the temperature inversion in the composition dependence for water-rich mixtures' isentropic compressibility.

Concerning the thermal conductivity of the "water-free" ionic liquid, it was found to be nearly temperature independent. For the mixture, the same behaviour as [C_2mim][CH_3SO_3] was found, with a maximum, especially at the higher temperatures, for $x_w > 0.998$. For the refractive index, the behaviour is similar to other systems, but shows a nearly zero excess refractive index for all temperatures and compositions. Very small values of the excess molar refractions were also found, with a minimum located at different compositions from those found for the excess volume.

These results seem to support the previous structural model proposed earlier [17,18], although data on electrical conductivity, viscosity, and diffusion are necessary to prove that this system is consistent with the previous ones, namely in the intermediary mole fraction zone. From these properties, viscosity is a very demanding property to assess the quality of a new heat transfer fluid, and for processing fluids in separation operations. However, there is no viscosity data for 1-Ethyl-3-Methylimidazolium Octanoate available in the literature. On handling, it looks that its viscosity at room temperature is slightly higher than that of 1-Ethyl-3-Methylimidazolium Acetate (around 198.4 mPa·s at 293.15 K and 25.75 mPa·s at 333.15 K [13]). The viscosity decreases drastically with small amounts of water, which is a good sign for a potential heat transfer fluid, and its applications in cellulose dissolving recommend the use of water mixtures, with lower viscosities also.

Regarding the application of models to estimate the thermal conductivity, namely Bridgman and Filaments model, it was unsuccessful, although some interesting features were found with the similarity of behaviour for the systems analysed, the difference between the sizes of molecules and the structure (packing, clusters, string of water molecules) being most probable drivers to correct the Filaments model. We hope to pursue this investigation with other IL + water systems in the future.

Results on refractive index of the mixtures show that it can be considered an ideal solution in the light of the optical properties measured and that the ideal molar refraction is additive in terms of the mole fractions, a result assumed in the past for molecules of simple molecular constitution, which is not the case for an ionic liquid.

To further evaluate the safety profile of [C_2mim][C_7H_{15}COO], it could be relevant to extend cytotoxicity studies to other human cell lines such as keratinocytes, which could help evaluate risks related to dermal exposure during handling. Such studies would complement existing data and inform safe design practices for ILs with potential industrial applications, as an environmentally acceptable green fluid.

In conclusion, the properties of 1-Ethyl-3-methylimidazolium octanoate, now reported, can pave the way for future applications in cellulose dissolving and extraction, as well as a heat transfer fluid, mixed with water.

CRediT authorship contribution statement

Rafael M. Almeida: Writing – original draft, Visualization, Investigation, Formal analysis, Data curation. **Elitsa Gadeva:** Investigation, Data curation. **Ângela F.S. Santos:** Writing – review & editing, Supervision, Methodology, Formal analysis, Conceptualization. **Rita Pacheco:** Writing – review & editing, Validation, Supervision, Resources, Methodology, Conceptualization. **Maria José V. Lourenço:** Visualization, Validation, Supervision, Resources, Methodology, Formal

analysis, Conceptualization. **Carlos Nieto de Castro:** Writing – review & editing, Validation, Supervision, Project administration, Investigation, Formal analysis.

Funding

This work was supported by Fundação para a Ciência e a Tecnologia, I.P., Portugal, through projects UID/QUI/00100/2019, and UIDB/00100/2020 (DOI: 10.54499/UIDP/00100/2020),

Declaration of competing interest

The authors declare that they have no known competing financial interests or personal relationships that could have appeared to influence the work reported in this paper.

Acknowledgments

RMA would like to thank CQE/FCT for his PhD research grant CQE - UI/BD/154429/2022. EG would like to thank the Mobility Program ERASMUS+, for the grant BG PLOVDIV 04, from 1st of May 2023 till 30th of September 2023, to work in Lisbon, for her Bachelor's Thesis.

Appendix A. Supplementary data

Supplementary data to this article can be found online at https://doi.org/10.1016/j.molliq.2025.128270.

Data availability

Data will be made available on request.

References

[1] D.R. MacFarlane, M. Kar, J.M. Pringle, Fundamentals of Ionic Liquids: From Chemistry to Applications, 1st ed., Wiley, 2017. ISBN: 978–3–527-33999-0.
[2] G. Kaur, H. Kumar, M. Singla, Diverse applications of ionic liquids: a comprehensive review, J. Mol. Liq. 351 (2022) 118556, https://doi.org/10.1016/j.molliq.2022.118556.
[3] X. Paredes, M.J. Lourenço, C. Nieto de Castro, W. Wakeham, Thermal conductivity of ionic liquids and IoNanofluids. Can Molecular Theory Help? Fluids 6 (3) (2021) 116, https://doi.org/10.3390/fluids6030116.
[4] J.M.P. França, C.A. Nieto De Castro, M.M. Lopes, V.M.B. Nunes, Influence of Thermophysical properties of ionic liquids in chemical process design, J. Chem. Eng. Data 54 (9) (2009) 2569–2575, https://doi.org/10.1021/je900107t.
[5] A.J. Greer, J. Jacquemin, C. Hardacre, Industrial applications of ionic liquids, Molecules 25 (2020) 5207, https://doi.org/10.3390/molecules25215207.
[6] P.G. Jessop, Searching for green solvents, Green Chem. 13 (2011) 1391–1398, https://doi.org/10.1039/C0GC00797H.
[7] Z. Yang, W. Pan, Ionic liquids: Green solvents for nonaqueous biocatalysis, Enzym. Microb. Technol. 37 (2005) 19–28, https://doi.org/10.1016/j.enzmictec.2005.02.014.
[8] A.R.P. Gonçalves, X. Paredes, A.F. Cristino, F.J.V. Santos, C.S.G.P. Queirós, Ionic liquids—a review of their toxicity to living organisms, Int. J. Mol. Sci. 22 (11) (2021) 5612, https://doi.org/10.3390/ijms22115612.
[9] J. Flieger, M. Flieger, Ionic liquids toxicity—benefits and threats, Int. J. Mol. Sci. 21 (17) (2020) 6267, https://doi.org/10.3390/ijms21176267.
[10] S. Taokaew, W. Kriangkrai, Recent Progress in processing cellulose using ionic liquids as solvents, Polysaccharides 3 (2022) 671–691, https://doi.org/10.3390/polysaccharides3040039.
[11] M.P. Vocht, R. Beyer, P. Thomasic, A. Müller, A. Ota, F. Hermanutz, M. R. Buchmeiser, High-performance cellulosic filament fibers prepared via dry-jet wet spinning from ionic liquids, Cellulose 28 (5) (2021) 3055–3067, https://doi.org/10.1007/s10570-021-03697-x.
[12] S.M. Green, M.E. Ries, J. Moffat, T. Budtova, NMR and rheological study of anion size influence on the properties of two imidazolium-based ionic liquids, Sci. Rep. 7 (1) (2017) 8968, https://doi.org/10.1038/s41598-017-09509-2.
[13] C.S.G.P. Queirós, X. Paredes, T.F.S. Avelino, D.E.N. Bastos, M. Ferreira, F.J. V. Santos, A.F. Santos, M.L.M. Lopes, M.J.V. Lourenço, H. Pereira, C.A. Nieto de Castro, The influence of water on the thermophysical properties of 1-ethyl-3-methylimidazolium acetate, J. Mol. Liq. 297 (2020) 111925, https://doi.org/10.1016/j.molliq.2019.111925.
[14] J.M. Choi, S.J. Oh, S.Y. Lee, J.H. Im, J.M. Oh, C.S. Ryu, H.C. Kwak, J.Y. Lee, K. W. Kang, S.K. Kim, HepG2 cells as an in vitro model for evaluation of cytochrome P450 induction by xenobiotics, Arch. Pharm. Res. 38 (5) (2015) 691–704, https://doi.org/10.1007/s12272-014-0502-6.
[15] I.M.S. Lampreia, C.A. Nieto de Castro, A new and reliable calibration method for vibrating tube densimeters over wide ranges of temperature and pressure, J. Chem. Thermodyn. 43 (2011) 537–545, https://doi.org/10.1016/j.jct.2010.11.002.
[16] F.E.B. Bioucas, S.I.C. Vieira, M.J.V. Lourenço, F.J.V. Santos, M.L.M. Lopes, C. A. Nieto de Castro, K. Massonne, [C2mim][CH3SO3] – A suitable new heat transfer fluid? Part 1. thermophysical and toxicological properties, Ind. Eng. Chem. Res. 57 (25) (2018) 8541–8551, https://doi.org/10.1021/acs.iecr.8b00723.
[17] F.E.B. Bioucas, C.S.G.P. Queirós, D. Lozano-Martín, M.S. Ferreira, X. Paredes, Â. F. Santos, F.J.V. Santos, M.L.M. Lopes, I.M.S. Lampreia, M.J.V. Lourenço, C. A. Nieto de Castro, K. Massonne, [C2mim][CH3SO3]—a suitable new heat transfer fluid? Part 2: Thermophysical properties of its mixtures with water, Ind. Eng. Chem. Res. 61 (5) (2022) 2280–2305, https://doi.org/10.1021/acs.iecr.1c02970.
[18] C.A. Nieto de Castro, A. Lamas, C. Magendran, R.M. Almeida, X. Paredes, Â. F. Santos, I.M.S. Lampreia, F.J.V. Santos, M.J.V. Lourenço, T.A. Graber, Thermophysical properties of 1-Ethyl-3-methylimidazolium Dicyanamide + water: understanding interactions and structure of ionic liquid + water systems, J. Chem. Eng. Data 69 (8) (2024) 2713–2734, https://doi.org/10.1021/acs.jced.4c00243.
[19] Â.F.S. Santos, M.-L.C.J. Moita, L.C.S. Nobre, I.M.S. Lampreia, Group-contribution to limiting partial molar isentropic compressions of small amphiphile molecules in water. The temperature effect, J. Chem. Thermodyn. 69 (2014) 157–164, https://doi.org/10.1016/j.jct.2013.10.013.
[20] I.M.S. Lampreia, Â.F.S. Santos, M.-L.C.J. Moita, L.C.S. Nobre, Thermodynamic study of aqueous 2-(isopropylamino)ethanol. A sterically hindered new amine absorbent for CO2 capture, J. Chem. Thermodyn. 81 (2015) 167–176, https://doi.org/10.1016/j.jct.2014.10.004.
[21] F. Spieweck, H. Bettin, H., Review: Solid and liquid density determination / Übersicht: Bestimmung der Dichte von Festkörpern und Flüssigkeiten, Tm - Tech. Mess. (1992) 59285–59292, https://doi.org/10.1524/teme.1992.59.78.285.
[22] Landolt-Börnstein: Neue Serie, Band 5, Molekul Akustik Temperatura Skala von 1990; PTB-Mitt 100, 1990, ISBN 978-3-540-85250-6, p. 2008 (n.d.). New edition, https://link.springer.com/book/10.1007%2F978-3-540-85251-3.
[23] M.L.V. Ramires, C.A. Nieto De Castro, Y. Nagasaka, A. Nagashima, M.J. Assael, W. A. Wakeham, Standard reference data for the thermal conductivity of water, J. Phys. Chem. Ref. Data Monogr. 24 (3) (1995) 1377–1381, https://doi.org/10.1063/1.555963.
[24] C.A. Nieto De Castro, M.J.V. Lourenço, Towards the correct measurement of thermal conductivity of ionic melts and Nanofluids, Energies 13 (1) (2019) 99, https://doi.org/10.3390/en13010099.
[25] X. Paredes, C.S.G.P. Queirós, F.J.V. Santos, A.F. Santos, M.S.C.S. Santos, M.J. V. Lourenço, C.A. Nieto de Castro, Thermophysical properties of 1-Hexyl-3-methylimidazolium bis(trifluoromethylsulfonyl)imide, [C6mim][(CF3SO2)2N]—new data, reference data, and reference correlations, J. Phys. Chem. Ref. Data Monogr. 49 (2020) 043101, https://doi.org/10.1063/5.0023160.
[26] D. Lozano-Martín, S.I.C. Vieira, X. Paredes, M.J.V. Lourenço, C.A. Nieto de Castro, J.V. Sengers, K. Massone, Thermal conductivity of metastable ionic liquid [C2mim][CH3SO3], Molecules 25 (2020) 4290, https://doi.org/10.3390/molecules25184290.
[27] K.N. Marsh, IUPAC, Recommended reference materials for the realization of physicochemical properties, Blackwell Scientific Publishing, Oxford, 1987.
[28] F. Sirbu, D. Dragoescu, A. Shchamialiou, T. Khasanshin, Densities, speeds of sound, refractive indices, viscosities and their related thermodynamic properties for n-hexadecane + two aromatic hydrocarbons binary mixtures at temperatures from 298.15 K to 318.15 K, J. Chem. Thermodyn. 128 (2019) 383–393, https://doi.org/10.1016/j.jct.2018.08.036.
[29] A.R. Ferraz, R. Pacheco, P.D. Vaz, C.S. Pintado, L. Ascensão, M.L. Serralheiro, Melanin: production from cheese Bacteria, chemical characterization, and biological activities, Int. J. Environ. Res. Public Health 18 (20) (2021) 10562, https://doi.org/10.3390/ijerph182010562.
[30] L.H.G.D. Medeiros, M.R.L.D. Silva, F.X. Feitosa, J.-L. Daridon, H.B. De Sant'Ana, Alkyl chain length effect on experimental density of three iodide anion-based ionic liquids at high-pressure and application of four group contribution estimation methods for ionic liquids density, J. Chem. Thermodyn. 195 (2024) 107294, https://doi.org/10.1016/j.jct.2024.107294.
[31] D. Santos, M. Santos, E. Franceschi, C. Dariva, A. Barison, S. Mattedi, Experimental density of ionic liquids and thermodynamic modeling with group contribution equation of state based on the lattice fluid theory, J. Chem. Eng. Data 61 (1) (2016) 348–353, https://doi.org/10.1021/acs.jced.5b00592.
[32] C.P. Fredlake, J.M. Crosthwaite, D.G. Hert, S.N.V.K. Aki, J.F. Brennecke, Thermophysical properties of imidazolium-based ionic liquids, J. Chem. Eng. Data 49 (4) (2004) 954–964, https://doi.org/10.1021/je034261a.
[33] A.P. Fröba, H. Kremer, A. Leipertz, Density, refractive index, interfacial tension, and viscosity of ionic liquids [EMIM][EtSO4], [EMIM][NTf2], [EMIM][N(CN)2], and [OMA][NTf2] in dependence on temperature at atmospheric pressure, J. Phys. Chem. B 112 (39) (2008) 12420–12430, https://doi.org/10.1021/jp804319a.
[34] M.G. Montalbán, C.L. Bolívar, F.G. Díaz Baños, G. Víllora, Effect of temperature, anion, and alkyl chain length on the density and refractive index of 1-Alkyl-3-methylimidazolium-based ionic liquids, J. Chem. Eng. Data 60 (7) (2015) 1986–1996, https://doi.org/10.1021/je501091q.
[35] A.S.L. Gouveia, L.C. Tomé, I.M. Marrucho, Density, viscosity, and refractive index of ionic liquid mixtures containing Cyano and amino acid-based anions, J. Chem. Eng. Data 61 (1) (2016) 83–93, https://doi.org/10.1021/acs.jced.5b00242.
[36] A.N. Soriano, B.T. Doma, M.-H. Li, Density and refractive index measurements of 1-ethyl-3-methylimidazolium-based ionic liquids, J. Taiwan Inst. Chem. Eng. 41 (1) (2010) 115–121, https://doi.org/10.1016/j.jtice.2009.07.002.
[37] NIST, Chemistry Webbook, SRD69. https://webbook.nist.gov/chemistry/, 2025, https://doi.org/10.18434/T4D303.

[38] W. Wagner, A. Kruse, Properties of water and steam: the industrial standard IAPWS-IF97 for the thermodynamic properties and supplementary equations for other properties, springer-Verlag, Berlin Heidelberg, 1998, https://doi.org/10.1007/978-3-662-03529-0.
[39] B. Jacobson, Intermolecular free lengths in liquids in relation to compressibility, surface tension and viscosity, Acta Chem. Scand. 5 (1951) 1214–1216, https://doi.org/10.3891/acta.chem.scand.05-1214.
[40] B. Jacobson, E.A. Halonen, C. Faurholt, Intermolecular free lengths in the liquid state. I. Adiabatic and isothermal Compressibilities, Acta Chem. Scand. 6 (1952) 1485–1498, https://doi.org/10.3891/acta.chem.scand.06-1485.
[41] M. Srinivasa Reddy, I. Khan, K.T.S.S. Raju, P. Suresh, B. Hari Babu, The study of molecular interactions in 1-Ethyl-3-Methylimidazolium Trifluoromethanesulfonate + 1-Pentanol from density, speed of sound and refractive index measurements, J. Chem. Thermodyn. 98 (2016) 298–308, https://doi.org/10.1021/acs.jced.3c00442.
[42] K.J. Jisha, Ramesh L. Gardas, Apparent molar properties and viscosity studies of ternary systems composed of model lignin and xylose in DBU based ionic liquid–DMSO solutions, J. Chem. Eng. Data 69 (10) (2024) 3357–3382, https://doi.org/10.1021/acs.jced.3c00442.
[43] W. Marczak, Jacobson's intermolecular free lengths in liquid mixtures – a thermodynamic approach, J. Chem. Thermodyn. 185 (2023) 107087, https://doi.org/10.1016/j.jct.2023.107087.
[44] M.C. Cumicheo, L.C.S. Nobre, A.F. Santos, I.M.S. Lampreia, M.S.C.S. Santos, F.J. V. Santos, H. Segura, C.A. Nieto De Castro, Thermophysical properties of 1-Butyl-1-methyl-pyrrolidinium Dicyanamide + H2O mixtures, J. Chem. Eng. Data 60 (12) (2015) 3766–3775, https://doi.org/10.1021/acs.jced.5b00944.
[45] R.M. Almeida, M.J.V. Lourenço, C. Nieto De Castro, The thermal conductivity of ionic liquids. Experiment and molecular interpretation, J. Mol. Liq. 397 (2024) 124123, https://doi.org/10.1016/j.molliq.2024.124123.
[46] P.W. Bridgman, The thermal conductivity of liquids, Proc. Am. Acad. Arts Sci. 59 (7) (1923) 141–169, https://doi.org/10.1073/pnas.9.10.341.
[47] F. Yebra, J. Troncoso, L. Romaní, Thermal conductivity of ionic liquids under pressure, Fluid Phase Equilib. 515 (2020) 112573, https://doi.org/10.1016/j.fluid.2020.112573.
[48] F. Yebra, J. Troncoso, L. Romaní, Thermal conductivity measurements for organic liquids at high pressure, J. Chem. Thermodyn. 142 (2020) 106005, https://doi.org/10.1016/j.jct.2019.106005.
[49] E. Postnikov, I.Yu. Pikalov, M. Chorażewski, Thermal conductivity of ionic liquids: recent challenges facing theory and experiment, J. Solut. Chem. 51 (2022) 1311–1333, https://doi.org/10.1007/s10953-022-01205-8.
[50] A. Melkikh, P. Skripov, Thermal conductivity of liquid mixtures: model of the dependence on concentration, Int. J. Thermophys. 44 (2023) 23, https://doi.org/10.1007/s10765-022-03125-7.
[51] J.C.R. Reis, I.M.S. Lampreia, A.F.S. Santos, M.L.C.J. Moita, G. Douhéret, Refractive index of liquid mixtures: theory and experiment, ChemPhysChem 11 (17) (2010) 3722–3733, https://doi.org/10.1002/cphc.201000566.
[52] M.L.C.J. Moita, B.G. Fialho, A.F.S. Santos, I.M.S. Lampreia, Exploring molecular interactions in two aqueous alkanolamines mixtures using refractive indices and molecular probes, J. Mol. Liq. 142 (2023) 122760, https://doi.org/10.1016/j.molliq.2023.122760.
[53] P. Brocos, A. Piñeiro, R. Bravo, A. Amigo, Refractive indices, molar volumes and molar refractions of binary liquid mixtures: concepts and correlations, Phys. Chem. Chem. Phys. 5 (2003) 550–557, https://doi.org/10.1039/B208765K.
[54] V.A. Arzumanian, O.I. Kiseleva, E.V. Poverennaya, The curious case of the HepG2 cell line: 40 years of expertise, Int. J. Mol. Sci. 22 (23) (2021) 13135, https://doi.org/10.3390/ijms222313135.
[55] X. Li, J. Ma, J. Wang, Cytotoxicity, oxidative stress, and apoptosis in HepG2 cells induced by ionic liquid 1-methyl-3-octylimidazolium bromide, Ecotoxicol. Environ. Saf. 120 (2015) 342–348, https://doi.org/10.1016/j.ecoenv.2015.06.018.
[56] Z. Zhang, J. Liu, X. Cai, W. Jiang, W. Luo, G. Jiang, Sorption to dissolved humic acid and its impacts on the toxicity of imidazolium based ionic liquids, Environ. Sci. Technol. 45 (4) (2011) 1688–1694, https://doi.org/10.1021/es103514s.
[57] R.F.M. Frade, A. Matias, L.C. Branco, C.A.M. Afonso, C.M.M. Duarte, Effect of ionic liquids on human colon carcinoma HT-29 and CaCo-2 cell lines, Green Chem. 9 (2007) 873–877, https://doi.org/10.1039/B617526K.
[58] J. Salminen, N. Papaiconomou, R.A. Kumar, J.-M. Lee, J. Kerr, J. Newman, J. M. Prausnitz, Physicochemical properties and toxicities of hydrophobic piperidinium and pyrrolidinium ionic liquids, Fluid Phase Equilib. 261 (1–2) (2007) 421–426, https://doi.org/10.1016/j.fluid.2007.06.031.
[59] V.R. Thamke, A.U. Chaudhari, S.R. Tapase, D. Paul, K.M. Kodam, In vitro toxicological evaluation of ionic liquids and development of effective bioremediation process for their removal, Environ. Pollut. 250 (2019) 567–577, https://doi.org/10.1016/j.envpol.2019.04.043.
[60] D.R.M. Passino, S.B. Smith, Acute bioassays and hazard evaluation of representative contaminants detected in great lakes fish, Environ. Toxicol. Chem. 6 (11) (1987) 901–907, https://doi.org/10.1002/etc.5620061111.